BINDER FREE SILICON ANODES FOR ADVANCED LITHIUM ION BATTERIES

A Project Report Submitted

as part of the requirements for the degree of

MASTER OF SCIENCE

Submitted by

RINI CHOUDHURY

Roll No. **CY14MSCST11014**

Under the Supervision of
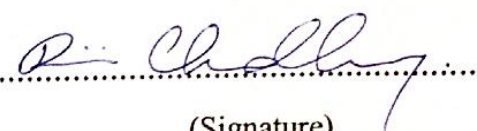
DR. SURENDRA K. MARTHA

भारतीय प्रौद्योगिकी संस्थान हैदराबाद
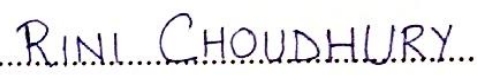Indian Institute of Technology Hyderabad

To the

DEPARTMENT OF CHEMISTRY

INDIAN INSTITUTE OF TECHNOLOGY HYDERABAD
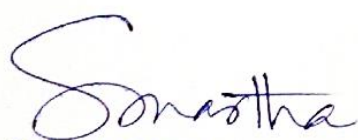
INDIA

APRIL, 2016

Declaration

I hereby declare that the matter embodied in this report is a result of investigation carried out by me in the Department of Chemistry, Indian Institute of TechnologyHyderabad under the supervision of **Dr.Surendra K. Martha**.

In keeping with general practice of reporting scientific observations, due acknowledgement has been made wherever the work described is based on the findings of other investigators.

(Signature)

RINI CHOUDHURY

(Student Name)

CY14MSCST11014

(Roll Number)

Dr. SURENDRA K. MARTHA
Assistant Professor
Department of Chemistry
Indian Institute of Technology Hyderabad

Signature of Supervisor

Dr.Surendra K. Martha

Department of Chemistry

Indian Institute of Technology, Hyderabad

Kandi, Sangareddy- 502285,

Telangana, India.

Approval Sheet

This thesis entitled **"Binder Free Silicon Anodes for Advanced Lithium Ion Batteries"** by Rini Choudhury is approved for the degree of Master of Science from Indian Institute of Technology Hyderabad.

Name and affiliation
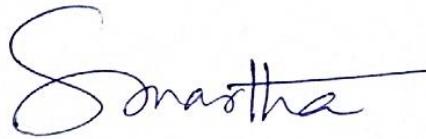
Examiner

Dr. M. Deepa
Head & Associate Professor
Department of Chemistry
Indian Institute of Technology Hyderabad
Kandi-502285, Sangareddy, Telangana, India

Name and affiliation

Examiner

Dr. SURENDRA K. MARTHA
Assistant Professor
Department of Chemistry
Indian Institute of Technology Hyderabad

Name and affiliation

Advisor

Name and affiliation

Chairman

Acknowledgements

Abstract

Silicon has emerged as an attractive anode material for Lithium Ion Batteries since it has a high theoretical capacity of 4200 mAh/g, corresponding to the formation of $Li_{22}Si_5$ alloy. Unlike graphite anodes which rely on intercalation and deintercalation of Li^+, silicon anodes depend on an alloying-dealloying process. However, the formation of Li-Si binary alloys involves volume modification of ~400%, and the repeated expansion and contraction during lithiation-delithiation leads to pulverization and consequent failure of the cell. To meet this challenge, we have designed binder-free silicon anodes that can circumvent the problem of pulverization. This work describes the synthesis of Si nanoparticles (NPs) by reverse micelle approach, followed by structural characterization of the material by X-Ray diffraction, Scanning Electron Microscopy and Raman Spectroscopy. The electrochemical performance of the Si active material as anode material for Lithium Ion Batteries was tested in two-electrode Swagelok type cells using galvanostatic charge-discharge cycling at different levels of depth-of-discharge, and also by impedance spectroscopy. Two approaches have been employed in the designing of the electrodes: firstly, the Si NPs were manually embedded on Cu foil as current collector by the application of pressure, and secondly, chitosan, polypyrrole-hydrogel and P-Pitch were used as novel binders in developing 3D electrode architecture on carbon fibre. The Si/Cu electrode fabricated via the first approach delivered specific capacity of above 700 mAh/g even after 150 cycles in the voltage range between 1.2 V and 0.05 V, and showed remarkable cycling stability at high rates for up to 350 cycles, due to the excellent adhesion of the silicon to the current collector and contribution of the entire electrochemically active electrode material to the capacity of the cell. Moreover, the low Si loading ensures sufficient gaps between particles to accommodate the volume modification of Si, thereby reducing the extent of pulverization. Pulverization and capacity decay have increased with low cut off voltages of 10 mV. The 3D carbon fiber electrode architecture developed using carbonized P-Pitch as a high-temperature binder and silicon active mass also delivers high initial capacities close to the theoretical value and further studies are under progress.

Contents

List of Figures:

List of Tables:

Chapter 1: Introduction to Lithium-Ion Batteries

1.1 Importance of Energy Storage

Energy is the lifeblood of the modern society.[1] The access to energy is very critical to the wealth, life style and image of every country. Today the world faces energy challenges on two main frontiers: shifting electricity production from burning fossil fuels to renewable energy sources, and moving ground transportation towards electrical propulsion, namely, using electric vehicles (EVs) instead of cars driven by internal combustion engines (ICEs). However, due to the intermittent nature of the known renewable energy sources such as solar, wind etc., there is a pressing need to design electrical energy storage systems that can efficiently store and deliver energy on demand, namely, batteries.

Batteries are energy storage devices that can convert the chemical energy stored in the active materials directly into electrical energy by means of an electrochemical oxidation-reduction reaction.[2] Where a rechargeable system is concerned, the battery is recharged by a reversal of the process. While the term 'battery' is commonly used, the basic electrochemical unit is the 'cell', which comprises a set of cathodes and anodes, electrolyte, separator, container and terminals. A battery is an arrangement of cells appropriately connected in series/parallel to provide the desired voltage and capacity.

Rechargeable batteries are produced in many different shapes and sizes, ranging from button cells to megawatt systems connected to stabilize an electrical distribution network. Several different combinations of electrode materials and electrolytes are used, including lead–acid, nickel cadmium (NiCd), nickel metal hydride (NiMH), lithium ion (Li-ion), and lithium ion polymer (Li-ion polymer) batteries.

The most surprising feature of today's battery industry continues to be the recent development and growth of Li-ion battery technology. Because of its superior energy density, the Li-ion battery is now the battery of choice in various mobile products such as portable computers, cellular telephones and camcorders.

1.2 Lithium Ion Battery: Importance and Historical Perspective

Lithium ion batteries (LIBs) have emerged as the most successful battery technology during the last two and half decades.[3] LIBs offer highest energy density of 120-160 Wh/kg (Fig 1.1) compared to other battery technologies such as lead-acid battery (30 Wh/kg), Ni based batteries (50-80 Wh/kg), and high open circuit voltage of 3.7 V. This is based on the fact that lithium is the lightest (atomic weight/equivalent weight of Li being 6.94 g/mol) metal as well as the most electropositive (-3.04 V vs. SHE) metal among other elements in the periodic table.
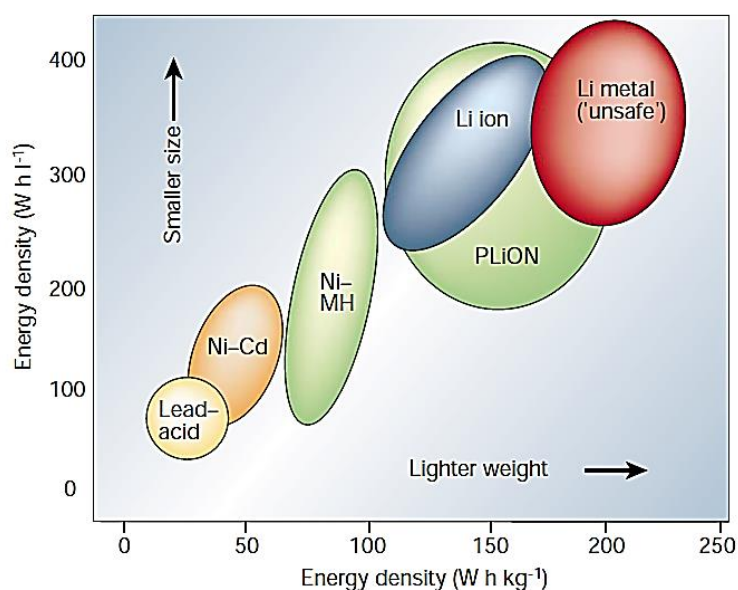
Figure 1.1 Comparison of the different battery technologies in terms of volumetric and gravimetric energy density.[4]

LIBs are light weight, compact, having a low self-discharge rate, high rate capability and moderate cycle life of about 1000 cycles. With such attractive performances, LIBs have conquered the consumer electronics market, making it the power source of choice not only for portable electronic devices such as laptops, cell phones and camcorders, but also in implantable devices, electric vehicles and Renewable Energy Plants.

In the early 1970s, research carried out on rechargeable lithium batteries by Professor Stanley Wittingham at the Exxon Laboratories in the US, established that lithium ions can be intercalated electrochemically into certain layered transition-metal sulphides, such as TiS_2. Based on this intercalation phenomena, the first rechargeable lithium cell was commercialized

in early 1980s by Moli Energy Corporation of Canada. The cell comprised a spirally wound lithium foil as the anode, a separator, a non-aqueous electrolyte and MoS_2 as the cathode.[5] During discharge, lithium ions are inserted into the van der Waals gap of TiS_2 with the concomitant reduction of Ti^{4+} to Ti^{3+}, while during charge, Li^+ are extracted from the van der Waals gap. The cell had a nominal voltage of 1.8 V and an attractive value of specific energy, which was 2 to 3 times greater than either lead-acid or nickel-cadmium cells. However, these cells failed in commercial applications due to serious safety problems associated with lithium metal, primarily due to the formation of dendrites. This paved way for the discovery of lithium-ion battery.

Subsequently, Yazami reported the reversible electrochemical intercalation of lithium in graphite, thus proposing graphite as anode for the replacement of lithium metal in lithium batteries.[6] The reversible intercalation of Li^+ between the graphene sheets of graphite, at an open circuit voltage (V_{oc}) of 0.2 V vs. Li/Li^+, was found to give a theoretical capacity of 372 mAh/g. Moreover, with slow charge-discharge rates the electrodes perform well and no dendrite formation is observed.

In 1980, J.B. Goodenough and his group at Oxford University introduced lithium cobalt oxide, Li_xCoO_2 (LCO), as a viable cathode material for LIBs, with lithium metal as the anode.[6] While the theoretical specific capacity of LCO is 274 mAh/g (based on one mole of lithium per formula unit), the practical capacity is limited to about 140 mAh/g, at V_{oc} of 3.7 V.

In 1991, SONY Company of Japan in collaboration with Goodenough developed world's first commercial rechargeable lithium ion battery by using LCO cathode and graphite anode, which forever changed the history of mobile devices. Following the commercialisation of the lithium ion battery in the 1990s, several improvements have helped to bring down the costs of the battery substantially. Even today LCO and graphite chemistries are used in many systems. However, the major disadvantage with LCO is that only half of the lithium can be extracted from the parent LCO compound, leaving safety as the biggest concern in many applications. Besides, LCO is not thermally stable and is bio-hazardous in nature.[7,8]

In 2005, SONY introduced Nexelion[TM], the first hybrid rechargeable lithium ion battery comprising a tin-based amorphous anode and a multi-stage composite cathode consisting of a mixture of cobalt, manganese, and nickel oxides such as $LiNi_{0.33}Mn_{0.33}Co_{0.33}O_2$. The battery

offered over 30% more capacity per volume as compared to conventional LIBs based on LCO and graphite.

During early 2007, A123 Systems of USA developed doped nano-phosphate (LiFePO$_4$-LFP) battery technology for hybrid electric vehicle applications with a focus on power, abuse tolerance, durability and cost. The products have low capacity loss and impedance growth over time and deliver calendar life of over 1500 cycles.

In the recent years extensive research is being conducted on Li- and Mn-rich compounds, such as Li$_{1.2}$Mn$_{0.55}$Ni$_{0.15}$Co$_{0.1}$O$_2$ which is a mixture of 2 compounds, viz. [Li$_x$Mn$_{1-x-2y}$Co$_y$Ni$_y$]O$_2$ and Li$_2$MnO$_3$. These materials promise a high discharge capacity of around 250 mAh/g at 4.7 V, which is within the limited voltage window of the electrolyte. Consequently, these materials provide almost double the energy density as compared to the above mentioned cathode chemistries, and may emerge as the candidate of choice for high-energy density LIBs for applications in electric vehicles. However, oxygen loss takes place at the high operating voltage (>4.5 V), and surface modifications are necessary to resolve this problem.[9, 10, 11]

Besides, the current research goal is also focused on achieving multielectron capacity in LIBs. The conversion material iron trifluoride (FeF$_3$) is also another attractive cathode material for LIBs which offers theoretical capacity of 712 mAh/g, almost 3-4 times energy density of currently used LCO or LFP based cathode materials.[12,13] However, poor kinetics of the electrochemical conversion reaction and issues of electronic and ionic conductivities have limited its optimal use. Further research is therefore necessary in order to fulfil the promise of high capacity conversion cathodes.

The pursuit for high capacity, high energy density lithium batteries has led to the emergence of the Lithium-air and Lithium-sulphur batteries as promising candidates, wherein a conversion process has replaced the conventional insertion processes. While reaction of Li with oxygen in the Li-air gives a capacity as high as 1200 mAh/g, the Li-S battery, assuming complete conversion, can yield energy density of upto 2500 Wh/kg. The research in these aspects are very new and may be the technology of the future.[14,15,16]

1.3 Working Principle of LIB

A lithium ion battery comprises anode and cathodes based on intercalation materials, such as graphite anode, a lithium transition metal oxide cathode ($LiMO_2$, eg. $LiCoO_2$), and an electrolyte consisting of a solution of a lithium salt (e.g. $LiPF_6$) in a mixture of organic carbonates (e.g. ethylene carbonate–dimethyl carbonate, EC–DMC)[17] imbedded in a separator felt. In the lithium-ion cell, the guest species (Li^+) are inserted and extracted without much structural modification of the host (graphite). The fully-charged negative plate is made of lithiated carbon, which is about 15% lithium by weight and has about the same electrochemical potential as metallic lithium. The discharged positive plate employs intercalation compounds, such as LCO.
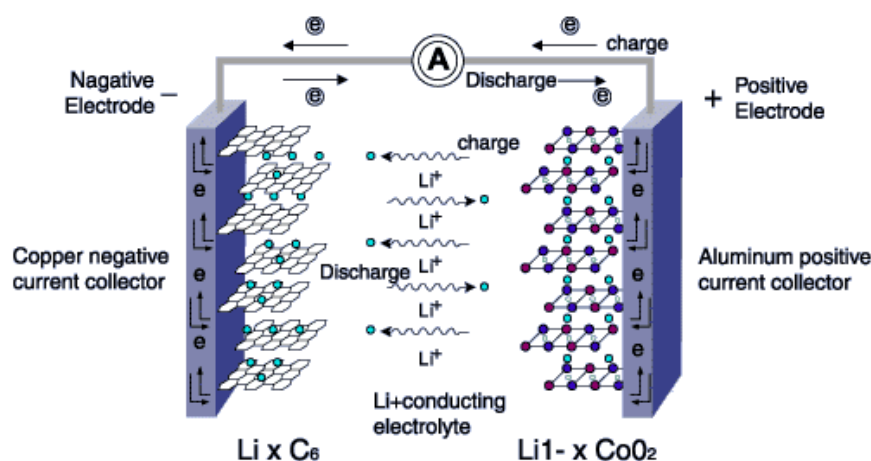
Figure 1.2 Schematic representation of a Li-ion cell.

At the positive electrode:

$$xLi^+ + xe^- + Li_{1-x}CoO_2 \underset{\text{Charge}}{\overset{\text{Discharge}}{\rightleftarrows}} LiCoO_2 \quad (E_c = 0.6 \text{ V vs. SHE}) {-}{-}{-}\cdot(1.1)$$

At the negative electrode:

$$LiC_6 \underset{\text{Charge}}{\overset{\text{Discharge}}{\rightleftarrows}} Li_{1-x}C_6 + xLi^+ + xe^- \quad (E_a = -3.06 \text{ V vs. SHE}) {-}{-}{-}\cdot(1.2)$$
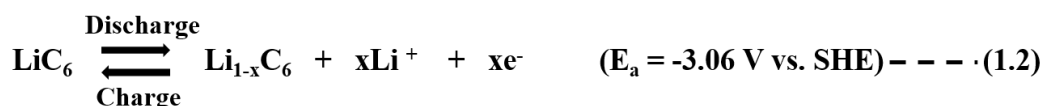
Accordingly, the net cell reactions during its charge-discharge process are:

$$LiC_6 + Li_{1-x}C_6 \underset{\text{Charge}}{\overset{\text{Discharge}}{\rightleftarrows}} Li_{1-x}CoO_2 + LiCoO_2 \quad (E_{cell} = 3.66 \text{ V}) {-}{-}{-}\cdot(1.3)$$
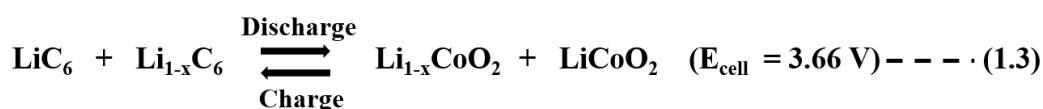
During charge, lithium ions get intercalated into the graphene layers of graphite and during discharge, they get back to the parent $LiMO_2$ compound. Lithium ions thus shuttle back and forth between the anode and cathode, without much structural change in the electrode materials- this phenomenon is often referred to as 'rocking chair' effect.

Ideally, the most advantageous combinations of cathode and anode are those that will be lightest, and will give highest cell voltage and capacity. However, for practical systems, other factors such as reactivity with other cell components, electrochemical stability, difficulty in handling, cost and safety factors must also be considered. Choice of anodes and cathodes depend on their efficiency as reducing agent and oxidizing agent, respectively, high Coulombic output, ease of fabrication, a suitable working voltage and cost. Some of the materials that are being explored as cathodes for LIBs are listed in Table 1.1.[18]

CATHODE MATERIALS		
Classification	**Material**	**Theoretical Capacity (mAh/g)**
Layered metal oxides	$LiCoO_2$	274
	$LiMnO_2$	285
	$LiNiO_2$	275
	$LiNi_{0.8}Co_{0.15}Al_{0.05}O_2$ **(NCA)**	279
	$LiNi_{1/3}Mn_{1/3}Co_{1/3}O_2$ **(NMC)**	280
Spinels	$LiMn_2O_4$	148
	$LiMn_{1.5}Ni_{0.5}O_4$	148
Olivines	$LiFePO_4$	170
	$LiMnPO_4$	171

Table 1.1 Commonly used active materials for cathodes in Lithium Ion Batteries.

The separator material is used to separate the anode and cathode electrodes mechanically but it must, however, be permeable to the electrolyte in order to maintain the desired ionic conductivity. Generally polyethylene, polypropylene based separators are used in LIBs.

Extensive research has been carried out to develop high capacity, high durability, and efficient anodes for LIBs. Anode materials are broadly classified into three categories, depending on their electrochemistry and reaction mechanisms. These include intercalation-deintercalation materials (which are mostly carbon-based materials), alloy-dealloy materials, and conversion materials like transition metal oxides. Examples of each category are given in Table 1.2.

Carbon-based materials, such as graphite, have been considered the most appropriate anode materials due to their low cost, ease of availability, thermal and chemical stability, and good working potential. Carbon-based materials may be further classified as *soft-carbons* (graphitizable carbons) and *hard carbons* (non-graphitizable carbons).[19] Examples of graphitizable carbon include Mesocarbon Microbead (MCMB), mesophase-pitch based carbon fibre (MCF), and vapour grown carbon fibre (VGCF). However, these materials have two major challenges—low specific capacity (372 mAh/g) and high-voltage hysteresis, which can limit their applications in advanced LIBs. Hard-carbons (such as CNTs), on the other hand, have higher reversible capacities of more than 500 mAh/g, but they suffer from low initial Coulombic efficiencies and low tap density.

Lithium titanate ($Li_4Ti_5O_{12}$) and titania (TiO_2) are the other examples of intercalation-based materials that are used as anodes for LIBs. While they offer excellent safety, low cost, good cycling stability (>1000 cycles) and high power capability, they do not ensure high capacity (theoretical value ~175 mAh/g for lithitum titanate and ~330 mAh/g for titania). Alloy-dealloy materials, in comparison to those discussed above, have higher specific capacities, ranging from ~780 mAh/g for SnO_2 to ~4200 mAh/g for Silicon based anodes. Conversion materials, which include transition metal oxides, suphides, phosphides and nitrides also exhibit high specific capacities in the range of 500-1000 mAh/g due to participation of a large number of electrons in the conversion processes. The electrochemistry of conversion-material based anodes involves the reduction or oxidation of the transition metal with the concomitant composition or decomposition of lithium compounds.[19] Some of the anode material candidates for LIBs have been listed in Table 1.2.

ANODE MATERIALS		
Classification	**Material**	**Theoretical Capacity (mAh/g)**
Intercalation-deintercalation materials	Graphite	372
	CNTs	1116
	TiO_2	330
	$Li_4Ti_5O_{12}$	175
Alloy-dealloy materials	Si	4212
	Ge	1624
	Sn	993
	Sb	660
	SnO_2	790
Conversion materials	Transition metal oxides: Fe_2O_3, Cu_2O/ CuO, NiO M_xZ_y (Z= S, P, N)	500-1200

Table 1.2 Commonly used active material for anodes in Lithium Ion Batteries.

Electrolytes for LIBs generally use non-coordinating anion salts such as lithium hexafluorophosphate ($LiPF_6$), lithium hexafluoroarsenate monohydrate ($LiAsF_6$), lithium perchlorate ($LiClO_4$), lithium tetrafluoroborate ($LiBF_4$) and lithium triflate ($LiCF_3SO_3$), in an organic solvent such as ethylene carbonate, dimethyl carbonate or diethyl carbonate. The electrolyte chosen must have high Li^+ conductivity, a wide electrochemical window and chemical stability, and must ensure retention of the electrode/electrolyte interface. Lithium arsenate salts are less preferred due to the toxicity of arsenic, and $LiClO_4$ tends to be explosive. $LiPF_6$ has emerged as the best choice because of high electrochemical stability of ~4.5V.[20,21,22]

1.4 Drawbacks and failure modes of Lithium Ion Batteries

While Li-ion battery technology delivers the best performance among the present battery technologies available in the market, it falls short of meeting all the requirements dictated by the vast range of applications related to renewable energy, hybrid and electric

vehicles. To compete with gasoline in the automotive industry, the energy delivered by LIBs should increase almost 15 fold in order to match that supplied by one litre of gasoline (3000 Wh l^{-1}) [1].

Energy density is the product of capacity and potential, and depends mainly on the capacity of the positive electrode. The key to increasing the energy density of LIBs lies, therefore, in the choice of suitable cathode materials: those that possess higher redox potentials (~5 V), or can reversibly intercalate more than one lithium ion per atom of the metal.

However, the relatively narrow stability domain (~ 0.8 V – 4.5 V) of the organic carbonate-based electrolyte prevents the use of high-voltage cathodes. In addition, the flammability of these organic electrolytes and their incompatibility with the environment and human health, pose serious hazards to safety. If the battery gets overheated, then the uncontrolled rise in temperature generates flammable gases. The separator tends to burn up, causing short circuit, and the cell may explode. This in turn may result in a cascading thermal runaway event, causing failure of multiple cells in the battery (Fig. 1.3).[23,24] Thus, there is a need for cathode materials with high operational voltages and capacity that can assure an increase in the energy density, as well as for suitable electrolyte media that may be compatible with the high voltage cathodes, especially during the course of their charge process.

1. Heating starts.
2. Protective layer breaks down.
3. Electrolyte breaks down into flammable gases.
4. Separator melts, possibly causing a short circuit.
5. Cathode breaks down, generating oxygen.

ANODE (CARBON)
PROTECTIVE LAYER
ELECTROLYTE (lithium salt in organic solvent)
SEPARATOR
CATHODE (LITHIUM METAL OXIDE)
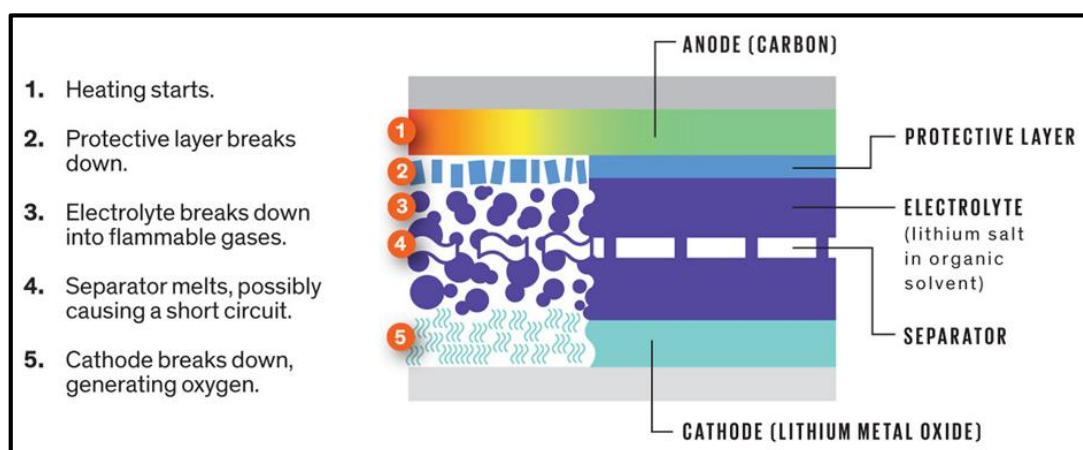
Figure 1.3 Thermal runaway in a lithium ion battery.

Another factor that is crucial to the battery performance is the formation of Solid Electrolyte Interphase (SEI), which is a culmination of the thermodynamic instability and

kinetic reactivity of the electrolyte. The electrolyte decomposes at the electrode surface on initial charging (lithiation) to form a passive layer which is electronically insulating yet provides significant ionic conductivity. This layer, which acts as an interphase between the metal and the solution, has the properties of a solid electrolyte and prevents further degradation of the electrolyte after the second charge.[25] The SEI comprises both inorganic components, which are normally salt degradation products (such as LiF), as well as organic components (eg. $(CH_2OCO_2Li)_2$, $ROCO_2Li$ and Li_2CO_3) which are partial or complete reduction products of the solvent of the electrolyte[26] (Fig 1.4). Typical SEI thicknesses range from ~20 Å to hundreds of angstroms.[27] Generally a good SEI is formed at a thermodynamic lithiation process.
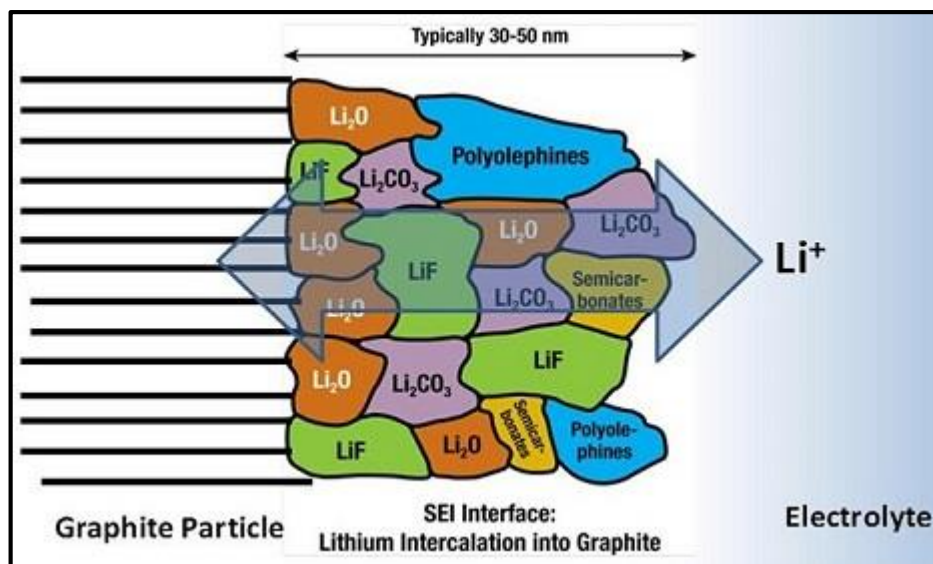
Figure 1.4a Diagrammatic representation of SEI formation
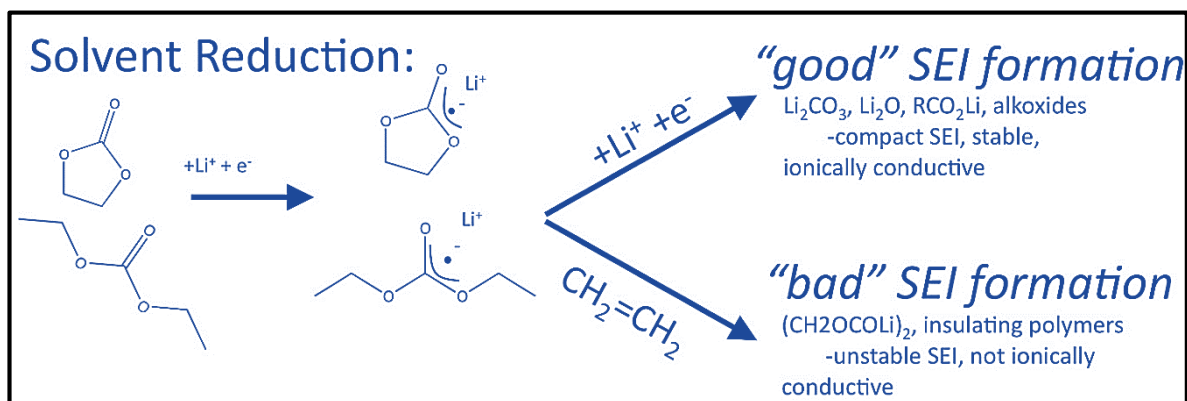
Figure 1.4b Reaction mechanism of SEI formation

In case of anodes, SEI formation occurs during the first lithiation, resulting an irreversible capacity loss of about 25%. An effective, stable SEI formation promotes good cycling life for the battery, preventing further electrolyte decomposition in subsequent cycles while allowing diffusion of Li^+ across the electrode/electrolyte interface. The formation of a surface film (SEI) has also been observed in case of cathodes[28], where, unlike anodes, the decomposition of the electrolyte is not limited to the first charge-discharge cycle; on the other hand, electrolyte decomposition occurs in successive cycles, resulting in a thicker and thicker SEI which prevents the electronic and ionic conduction, causing cell failure.

Battery performance depends significantly on the composition, thickness and compactness of the SEI. SEI dissolve and/or evolve during cycling. The formation of a stable SEI at anode attains even more importance during cycling at high rates and at deeper depth of discharge.[29] It is thus evident that SEI formation is crucial to the electrochemical performance and cycling stability of lithium ion batteries, and the lack of a dense, stable interphase at the electrode/electrolyte interface is often responsible for capacity loss and poor cyclability.

Besides cathodes and electrolytes, another limiting factor for the Li-ion battery is the graphite anode. Graphite remains the popular choice for commercial LIBs, with its good mechanical stability, electrical conductivity and high Li^+ diffusivity, coupled with ease of availability and low delithiation potential (0.2 V vs. lithium metal). However, only one Li atom can be intercalated per six atoms of carbon, resulting in a theoretical capacity of only 372 mAh/g (its practical capacity is ~330 mAh/g). Moreover, if a stable SEI is not formed, exfoliation of graphite may take place due to co-intercalation of solvent molecules, along with Li^+, between the graphene sheets.[30] This in turn would lead to structural degradation, exposing fresh surfaces of graphite to the electrolyte and thereby resulting in further electrolyte decomposition.

These factors have made it imperative to look beyond carbon-based materials for the next generation Li-ion battery technology. While alloy-anodes can have extremely high capacities, they are notorious for their large volume modification (300-400 %) during lithiation and delithiation. This volume change can lead to destruction of the SEI, resulting in continuous electrolyte decomposition which in turn can accelerate cell failure. Alloy anodes also suffer from high irreversible capacities, loss of active material and poor cycling stability.

1.5 Current Status of Lithium-Ion Batteries

Extensive research in developing advanced lithium ion batteries has revealed that more promising results may be obtained by using known active materials in their nanostructured form, as this helps to a considerable extent in overcoming the problems associated with volume expansion, poor ion transport, capacity fading, and low Coulombic efficiency. Nano-size structures with tailored morphology play a pivotal role in making efficient energy storage devices.

The advantages of incorporating nanomaterials in lithium ion batteries may be listed as follows:

- Nanostructured morphologies allow for better accommodation of the large volume changes without the initiation of fracture that can occur in bulk or micron-sized materials.[31]
- The high surface area to volume ratio increases the sites available for Li^+ storage as well as the contact area with the electrolyte, leading to high Li^+ flux across the electrode/electrolyte interface.
- They enable the occurrence of reactions that cannot take place in bulk or even micrometre sized particles, for example, reversible lithium intercalation into mesoporous β-MnO_2 without destruction of the rutile.[32]
- The nanoscale dimensions lead to a significant increase in the rate of lithium diffusion because of the short distances for lithium-ion transport within the particles.
- Electron transfer rates are enhanced.

However, there are also some potential disadvantages associated with the development of nanoelectrodes. These include the increased possibility of undesirable side reactions due to the high electrode/electrolyte surface area, difficulty in synthesizing nanoparticles and controlling their dimensions, and reduced volumetric energy density due to lowered density of nanopowders or inferior packing of the material.[33,34]

With these advantages and disadvantages in mind, efforts have been devoted to the development of nanostructured electrodes for LIBs to overcome the problems that limit their

electrochemical performance. Some of the approaches adopted for the same may be summarised in Fig. 1.5.
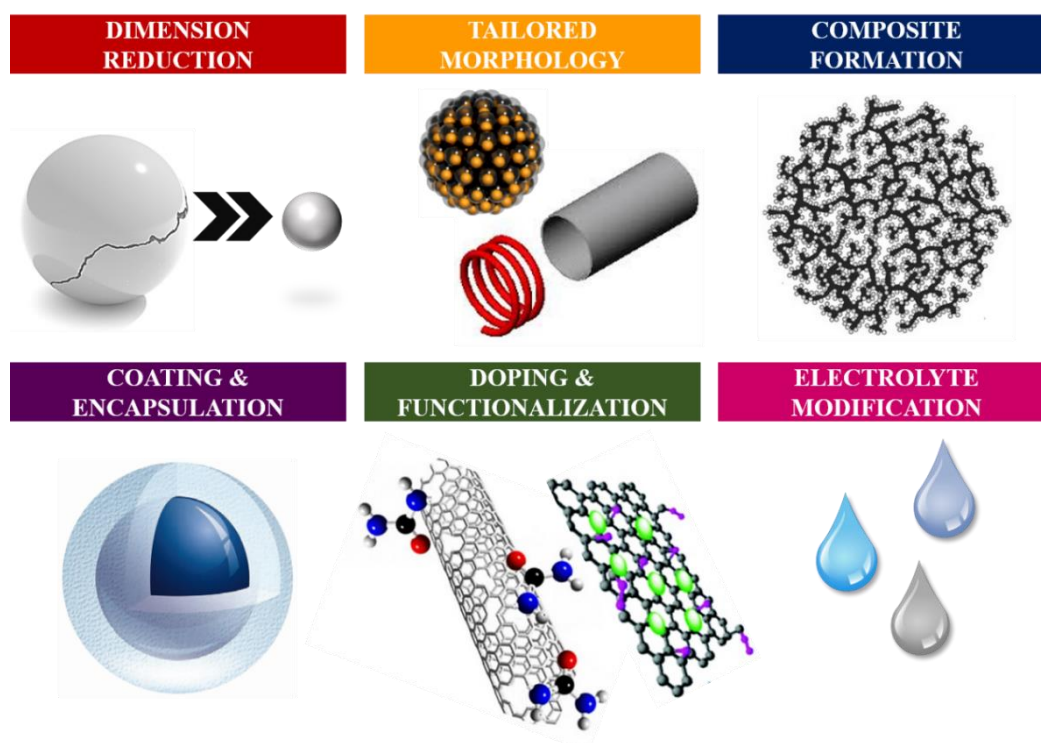
Figure 1.5 Approaches for the realization of advanced Lithium Ion Batteries.

Using new synthetic processes of nanotechnology, one can create millions of identical nanostructures with shapes tailored to transport electrons rapidly to and from very large surface areas, thereby acting as efficient energy storage devices. The current challenge is geared towards developing high voltage $LiNiPO_4$, $LiCoPO_4$, silicates or high capacity excess Lithia compounds as cathode materials which can operate at voltages as high as 5.2 V and be thermally stable.[35,36] At such high potentials the anodic stability of the electrolyte solutions will be key factor and its operation for EV at low temperature could be crucial. Standard electrolyte solutions do not necessarily meet this challenge. Hence the possible use of ionic liquids in Li ion batteries as a solution to both limited anodic and thermal stability could be beneficial.[37] The combinations of materials, processes, and structures to optimize both energy and power density taken together, have a real promise for building next-generation technology. Besides graphite, silicon and tin based alloy anodes have emerged as anode materials for next generation LIBs.[38]

Based on the current challenges, our research is focused on developing high performance silicon anodes for high energy density lithium ion batteries. Silicon has high theoretical capacity of ~4200 mAh/g, and could pave the way for future LIBs with enhanced electrochemical performance and longer cycle life. We have designed binder-free Silicon anodes in order to fulfil the promise of high capacity while circumventing the problems traditionally associated with silicon-based anodes.

References:

1. J.M. Tarascon, *Phil. Trans. R. Soc. A*, 2010, **368**, 3227–3241

2. Linden, D., & Reddy, T. B., 2002, *Handbook of batteries*. New York: McGraw-Hill

3. V. Etacheri, R. Marom, R. Elazari, G. Salitra and D. Aurbach, *Energy Environ. Sci.,* 2011, **4**, 3243–3262

4. J.M. Tarascon and M. Armand, *Nature,* 2001, **414**, 359

5. M.S. Wittingham, *Science*, 1976**, 192**, 1126-1127

6. R. Yazami and P.Touzain, *J. Power Sources*, 1983, **9**, 365-371

7. M. S. Wittingham, *Chem. Rev.* 2004, **104**, 4271−4301

8. C.-H Doh, D.-H. Kim, H.-S. Kim, H.-M. Shin, Y.–D. Jeong, S.-I Moon, B.-S. Jin, S. W. Eom, H.-S. Kim, K.-W. Kim, D.-H. Oh, A. Veluchamy, *J. Power Sources*, 2008, **175**, 881–885

9. D. Mohanty, S. Kalnaus, R. A. Meisner, K. J. Rhodes, J. Li, E. A. Payzant, D. L. Wood III and C. Daniel, *J. Power Sources*, 2013, **229**, 239–248

10. C. M. Julien, A. Mauger, K. Zaghib and Henri Groult, *Inorganics,* 2014, **2**, 132-154

11. S. K. Martha, J. Nanda, Y. Kim, R. R. Unocic, S. Pannala and Nancy J. Dudney, *J. Mater. Chem. A*, 2013, **1**, 5587-5595

12. T. Li, L. Li, Y. L. Cao, X. P. Ai and H. X. Yang, *J. P-hys. Chem. C,* 2010, **114**, 3190–3195

13. L. Li, F. Meng and S. Jin, *Nano Lett.*, 2012, **12**, 6030–6037

14. G. Girishkumar, B. McCloskey, A. C. Luntz, S. Swanson and W. Wilcke, *J. Phys. Chem. Lett.*, 2010, **1**, 2193–2203

15. H.-G. Jung, J. Hassoun, J.-B. Park, Y.-K. Sun and B. Scrosati, *Nat. Chem.,* 2012, **4**, 579–585

16. L. F. Nazara, M. Cuisiniera and Q. Panga, *MRS Bulletin*, 2014, **39**, 436-442

17. B. Scrosati, *Electrochim. Acta*, 2000, **45**, 2461–2466

18. N. Nitta, F. Wu, J.T. Lee and G. Yushin, *Materials Today*, 2015, **18**, 252-264.

19. S. Goriparti, E. Miele, F. D. Angelis, E. D. Fabrizio, R. P. Zaccaria, C. Capiglia, *J. Power Sources*, **2014**, *257*, 421-443

20. D. Aurbach, Y. Talyosef, B. Markovsky, E. Markevich, E. Zinigrad, L. Asraf, J. S. Gnanaraj and H.-J. Kim, *Electrochim. Acta*, 2004, **50**, 247–254

21. K. Xu, *Chem. Rev.*, 2004, **104**, 4303–4418

22. V. Aravindan, J. Gnanaraj, S. Madhavi and H.-K. Liu, *Chem. Eur. J*, 2011, **17**, 14326–14346

23. P.G. Balakrishnan, R. Ramesh and T. Prem Kumar, *J. Power Sources*, 2006, **155**, 401–414

24. Q. Wang, P. Ping, X. Zhao, G. Chu, J. Sun and C. Chen, *J. Power Sources*, 2012, **208**, 210–224

25. E. Peled, *J. Electrochem. Soc.*, 1979, **126**, 2047-2051

26. P. Verma, P. Maire and P. Novák, *Electrochim. Acta*, 2010, **55**, 6332–6341

27. K. Edström, M. Herstedt and D. P. Abraham, *J. Power Sources,* 2006, **153**, 380–384

28. K. Edström, T. Gustafsson and J.O. Thomas, *Electrochim. Acta,* 2004, **50**, 397–403

29. N. Ogihara, Y. Igarashi, A. Kamakura, K. Naoi, Y. Kusachi and K. Utsugi, *Electrochim. Acta*, 2006, **52**, 1713-1720

30. J.O. Besenhard, M. Winter, J. Yang and W. Biberacher, *J. Power Sources*, 1995, **54**, 228-231

31. C. K. Chan, H. Peng, G. Liu, K. Mcilwrath, X. F. Zhang, R. A. Huggins and Y. Cui, *Nat. Nanotechnol.,* 2008*, **3**, 31 - 35

32. F. Jiao and P. G. Bruce, *Adv. Mater.*, 2007, **19**, 657-660

33. P. Bruce, B. Scrosati and J.M. Tarascon, *Angew. Chem. Int. Ed.*, 2008, **47**, 2930 – 2946

34. A.S. Aricò, P. Bruce, B. Scrosati, J.M. Tarascon and W.V. Schalkwijk, *Nat. Mater.*, 2005, **4**, 366-377

35. B. Xu, D. Qian, Z. Wang, Y. S. Meng, *Mater. Sci. Eng. R-Rep.*, 2012, **73**, 51–65

36. A. Manthiram, *J. Phys. Chem. Lett.,* **2011**, *2*, 176–184

37. B. Scrosati, J. Hassouna and Y.-K. Sun, *Energy Environ. Sci.*, 2011, **4**, 3287-3295

38. W.-J. Zhang, *J. Power Sources*, 2011, **196**, 13–24

Chapter 2: Binder-Free High Performance Silicon Anodes for Advanced Lithium Ion Batteries

Although graphite has been the most popular choice as anode in commercial LIBs, it has a specific capacity of only 372 mAh/g and also suffers from several disadvantages, such as poor cyclability and Solid Electrolyte Interface (SEI) formation. This relatively low capacity limits the overall energy density of the cell. To develop high-energy density lithium ion batteries, extensive research is in progress with a view to finding and developing higher capacity electrode materials.

Silicon is of great interest since it has ten times higher specific capacity than traditional graphite anodes. An ideal anode material should possess high gravimetric and volumetric capacities, low potential against cathode material, light weight, good cycle life and should be cost-efficient. Silicon and its derivatives fulfil these criteria, making them highly attractive alternatives to traditional carbon-based anodes for the realization of future generation of LIBs. The main advantages of Silicon being an attractive anode material are as follows:

➢ Silicon has both the highest gravimetric capacity **(4200 mAh/g, $Li_{22}Si_5$)** and volumetric capacity **(9786 mAh cm^{-3})** among the anode material candidates[1,2]

➢ Lithiation potential of silicon is almost close to graphite i.e. 0.4 V vs. Li/Li^+.[3] This moderate potential averts the safety concern of lithium deposition as with graphite anodes (~0.05 V vs. Li)[4]

➢ Si, being the second most abundant element on earth, is inexpensive and eco-friendly

In spite of its promise of high specific capacity, there are certain fundamental challenges to the use of silicon as a viable anode material in LIBs. These may be outlined as follows:

i. **Material pulverization:** The large volume expansion/contraction (~400%) during charge-discharge due to alloying of Li with silicon induces large stress, leading to pulverization of Si which, in turn, causes loss of electrical contact with the current collector and eventually capacity fade.

ii. **Morphology and volume change of the whole Si electrode:** The total volume of the whole Si anode also increases and decreases upon lithiation and delithiation, leading to its detachment from the current collector and resulting in failure of the cell.

iii. **SEI formation:** When the potential of the Si anode is below ~1 V versus Li/Li$^+$, the organic electrolyte decomposes at the electrode surface to form SEI layer. The SEI plays a major role in regulating the alloying kinetics and in electron transport at the surface. In case of Si, the volume modification makes the formation of a stable SEI extremely difficult. The SEI formed in the lithiated state can be broken as the particle shrinks during delithiation, thus re-exposing the fresh Si surface to the electrolyte. This, in turn, results in thicker and thicker SEI upon charge/discharge.
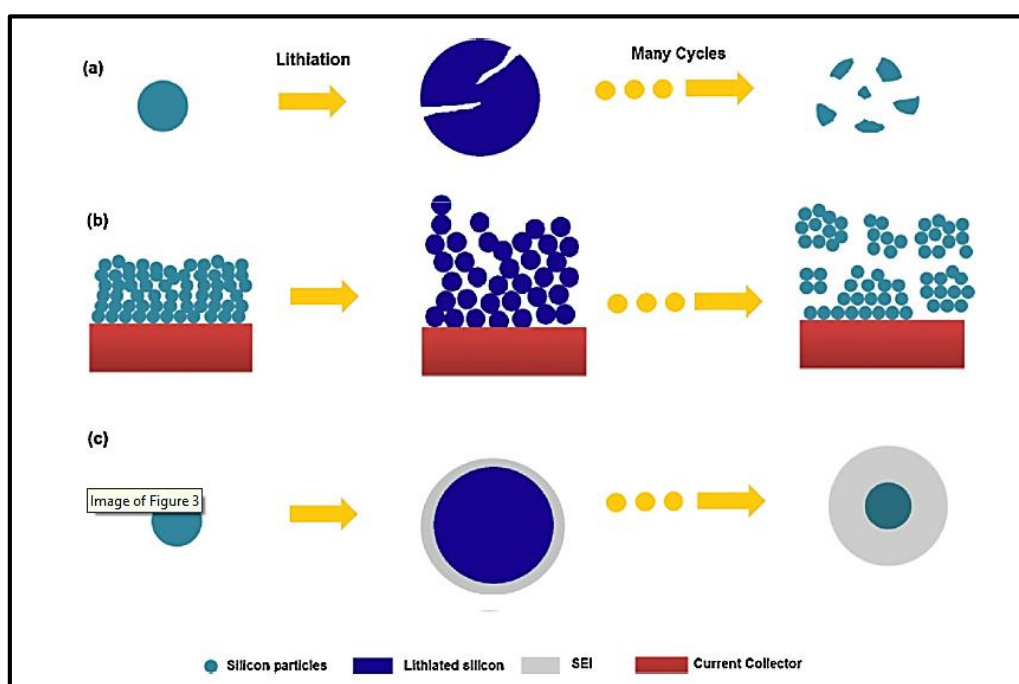
Figure 2.1 (a) Material Pulverization; **(b)** Morphology and volume change of the entire Si electrode; **(c)** Continuous SEI growth [5]

However, it has been shown that nanostructured silicon battery anodes circumvent these issues as they can provide enough free space to accommodate expansion during alloying, thus minimizing the strain that would otherwise lead to pulverization. In addition, nanoscale dimensions provide good electronic contact and reduce lithium diffusion distance, thereby enhancing rate capability and specific capacity.

Various nanostructured morphologies of silicon have been explored over the years with a view to addressing the challenge of volume modification. These include *nanowires and nanotubes* [6-11], *interconnected hollow nanospheres*[12], *thin films*[13], *vesica*[14] and *nanoparticles*[15]. In addition, some electrode designs incorporate carbon based materials to enhance the conductivity while also addressing the basic issue of pulverization. Most of these nanoscale designs incorporate pores or voids to accommodate the volume modification, or utilise the high surface area-to-volume ratio to allow for stress relaxation[16]. Moreover, binder less electrode architectures are becoming increasingly popular as these facilitate efficient charge transport and also eliminate the need for binders, which would otherwise contribute extra weight and add to the resistivity of the cell [6, 17-21].

Some innovative nanostructured electrodes that have been developed to alleviate the pulverization of Si in multifaceted ways, thereby displaying improved electrochemical performances, have been briefly described herein.

- **Carbon-Silicon core-shell nanowires**[22]**:** Using this composite anode, capacity of ~2000 mAh/g, high Coulombic efficiency of 90% for the first cycle, 98-99.6% for following cycles and about 80 charge-discharge cycles have been achieved.
  Carbon core experiences less structural stress or damage during lithium cycling and can function as a mechanical support and an efficient electron conducting pathway.

- **Helical Si/SiO$_x$ core-shell nanocoils on bulk Si (C-coated, urchin-like composite)**[23]**:** Capacity of ~1600 mAh/g, 70 charge-discharge cycles; high volumetric capacity of ~3780 mAh/cc compared to bulk Si (~2720 mAh/cc) have been achieved by using this composite anode.
  3D network formed by the protruding spines improve electrode conductivity, empty space formed between the spines and the inner Si core facilitates contact of active materials with electrolyte and enhances Li$^+$ transport, SiO$_x$ acts as buffer layer, and C coating improves conductivity & alleviates volume change.

- **Gold-coated porous Si films attached to bulk Si**[24]**:** Specific capacity over 3000 mAh/g for over 50 charge–discharge cycles, and 2500 mAh/g for over 75 cycles with coulombic efficiencies over 95% have been obtained.

Gold coating hinders the structural degradation in the porous silicon as it undergoes volume expansion during lithiation.

- **Aligned Si-CNT Sheets**[25]**:** Initial charge and discharge capacity of 2270 and 1801 mAh/g at 50 mA/g current density are obtained. The electrodes retain about 1350 mAh/g capacity after 45 cycles.
  No binder, no current collector was used during the electrode fabrication. Aligned CNT structure allows for controlled volume expansion of Si.

- **Pomegranate-inspired Si-C nanoscale design**[26]**:** Single Si nanoparticles are encapsulated by a conductive carbon layer by this approach; these hybrid nanoparticles are then encapsulated in thicker carbon pouches. Initial capacity of 2350 mAh/g at C/20 rate and 97% capacity retention after 1,000 cycles have been achieved for these electrodes.
  In these electrodes, the volume expansion is internally accommodated, SEI is spatially confined, and carbon coating enhances conductivity which in turn results in improved cyclability.

- **Adaptable Silicon-Carbon nanocables sandwiched between reduced graphene oxide sheets**[27]**:** Encapsulation of Si NWs with overlapped graphene (G) sheaths and reduced graphene oxide (RGO) overcoats results in an improved capacity of 1600 mAh/g, 80% capacity retention after 100 cycles, and superior rate capability.
  In these electrodes, graphene sheaths prevent direct exposure of Si to the electrolyte; flexible and conductive RGO sheets accommodate volume expansion during lithiation and delithiation.

- **Spheroidal carbon-coated Si nanocomposite**[28]**:** Initial lithiation capacity of 2600 mAh/g and a delithiation capacity of 1857 mAh/g achieved for these active materials (i.e. 44% Si and 56% C); maintained high capacity and reversibility even after 20 cycles.
  Amorphous carbon coating provides high electronic conductivity, buffers the large volume changes, and also avoids possible agglomeration of uniformly distributed Si particles.

To summarize, the primary problem associated with silicon anodes is the pulverization that occurs as a result of volume expansion and contraction during lithiation and delithiation, respectively. This pulverization includes fracturing of individual particles and also the detachment of the material from the current collector due to stress induced by the alloying-dealloying process at the level of the entire electrode. The goal, therefore, is to design an electrode that will improve capacity retention and cycling stability by accommodating the volume modification. In this work, we have tried to address this challenge by developing binder-free Silicon anodes for the realization of advanced lithium ion batteries. Both copper foil and carbon fibre have been used as current collectors for this purpose. Electrode preparation methods include pressure-embedding Si active material onto copper foil, and developing 3D electrode architecture with a series of different binders such as chitosan, polypyrrole hydrogel, as well as high-temperature carbon binders such as pitch, to enhance conductivity and reduce capacity loss due to pulverization.

2.1 Synthesis and structural characterization of Silicon nanoparticles

2.1(a) Experimental: The Si NPs are synthesized in reversed micelles of $N(C_8H_{17})_4$ Br (N-octyl ammonium bromide) in toluene, via a short synthetic route (< 3hr) with mild silicon sources and high yields up to gram-scale.[29] The process is schematically depicted in Figure 2.1.1.
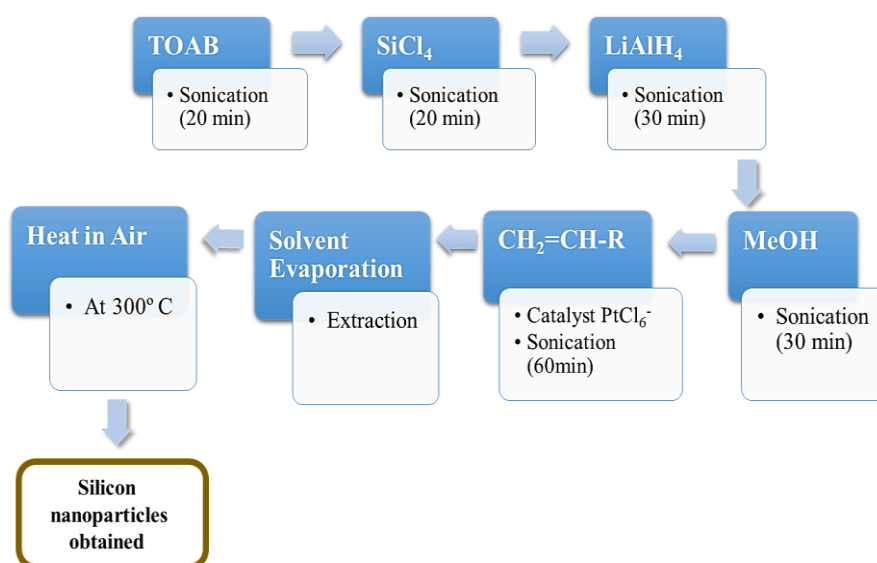
Figure 2.1.1 Schematic for the synthesis of silicon nanoparticles.

Powder XRD measurements were performed using Panalytical X'Pert PRO (reflection θ:θ geometry, Cu Kα radiation). The diffraction data were collected at a step size of 0.0170 over a 2θ range from 10 to 60º. The morphology and particles size were determined by field emission scanning electron microscopy, using Carl Zeiss AG Supra 40 FE-SEM instrument, equipped with energy-dispersive X-ray microanalysis systems. The samples were also characterized by Raman spectroscopy using a Bruker Senterra Raman microscope spectrometer.

2.1(b) Results and Discussion: Figure 2.1.2(a) shows the powder XRD pattern of the as-prepared Silicon nanoparticles. The XRD peaks are characteristics for a crystalline silicon sample having a face-centred cubic lattice. No impurity phases were detected.
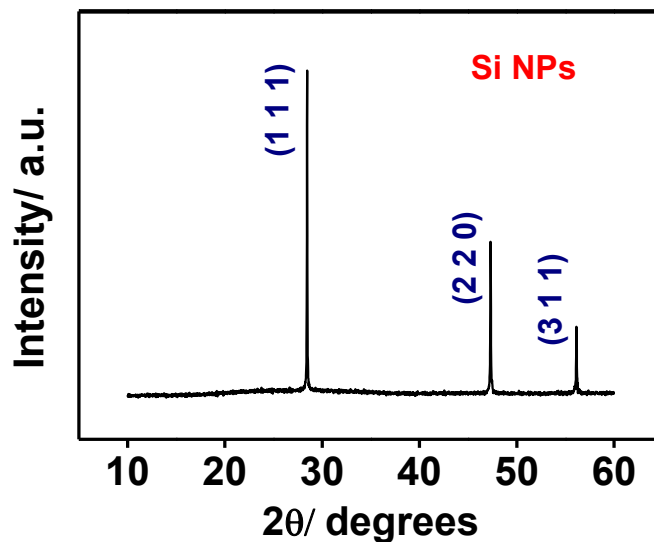

Figure 2.1.2 (a) X-ray diffraction pattern of the as-synthesized silicon nanoparticles.

Figure 2.1.2 (b) presents a typical Raman Spectrum of the silicon nanoparticles. The sharp, intense peak at 510 cm^{-1} is characteristic of crystalline Si-Si stretching band. The weak band at 928 cm^{-1} corresponds to the second order Raman signal for silicon.
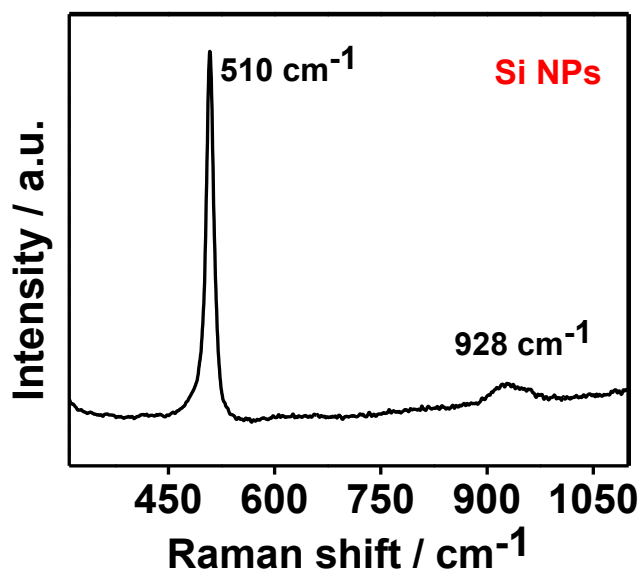

Figure 2.1.2 (b) Raman shift in cm^{-1} of the as-synthesized silicon nanoparticles.

Figure 2.1.2 (c) shows the FESEM image of the as-prepared silicon nanoparticles. The silicon particles have spherical morphology, with particle sizes in the range of 25-50 nm.
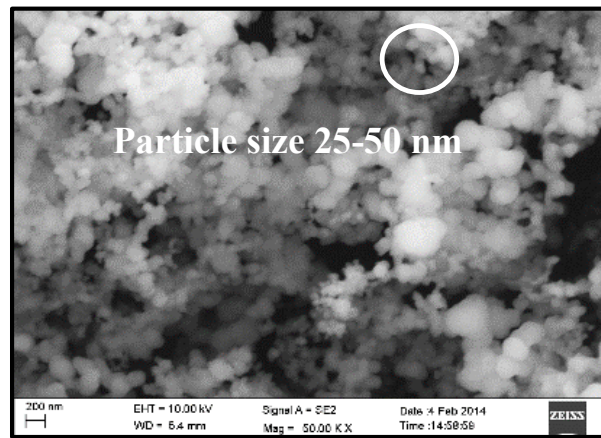

Figure 2.1.2 (c) SEM image of the as-synthesized silicon nanoparticles.

2.2 Electrochemical performance of Silicon

2.2.1 Testing actual capacity of pure silicon on copper foil

2.2.1(a) Experimental: Electrodes were prepared by embedding the as synthesized silicon nanoparticles by pressure onto copper foil as the current collector, without using any additional conductive carbon diluents or organic binders such as Polyvinylidene fluoride (PVDF). The electrodes were then punched to desired size (circular disks area ~ 1 cm^2) and weighed using a semi-micro balance from Sartorius AG. The weight of the active material was determined to be 0.05 mg. Scanning Electron Microscopy and Energy Dispersive X-ray Spectroscopy (EDS), were performed using a Carl Zeiss FESEM instrument, to observe the distribution of the Silicon NPs on the copper foil.

Another set of electrodes were prepared by slurry method, wherein the active material (Si NPs, 50 wt. %), high surface area active carbon, ACS 2500 (40 wt%) and binder (10 wt% PVDF dissolved in N-methyl-2-pyrrolidone, NMP) were mixed thoroughly by a vortex mixture to form a slurry. This slurry was then coated onto copper foil using the doctor-blade technique. The as-prepared conventional Si electrode was then dried under vacuum at 90 °C, punched into 1 cm^2 size electrodes and weighed. The weight of the active material was about 1.6 mg.

The electrochemical performance of the as-prepared Si/Cu electrodes was evaluated in two-electrode Swagelok cells with pure lithium foil as the counter electrode and PP/PE/PP trilayer separator (Celgard Inc.). The electrolyte comprised 1.2 M LiPF$_6$ dissolved in a mixture of ethylene carbonate (EC) and dimethyl carbonate (DMC) (1:1 by volume). The cells were assembled in a glove box (MBraun Inc.) filled with pure argon gas. Galvanostatic charge–discharge cycling was carried out using a multichannel battery tester from Arbin Instruments Inc. within the operating voltage range of 1.2 to 0.05 V, and 1.2 V to 0.01 V, respectively.

2.2.1(b) Results and discussion: Figure 2.2.1 (a) shows the SEM image of the Si/Cu electrode. It gives the distribution of the active material on the copper foil. Particles are distributed randomly, with sufficient spaces between them. The distribution of the silicon nanoparticles is seen to be more concentrated in certain regions on the copper foil, and less concentrated in others.
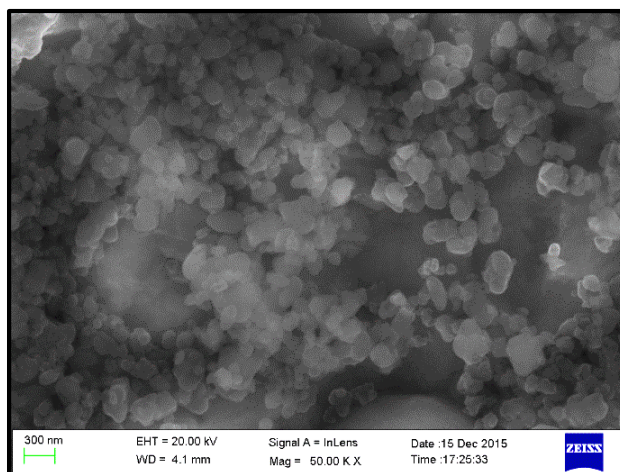
Figure 2.2.1 (a) SEM image of the as-prepared Si/Cu electrode.

Figure 2.2.1 (b) is the EDS examination of the as-prepared electrode. It shows that Si and Cu are the major components of the electrode. The presence of oxygen indicates that the Si NPs and Cu foil may be slightly oxidized.
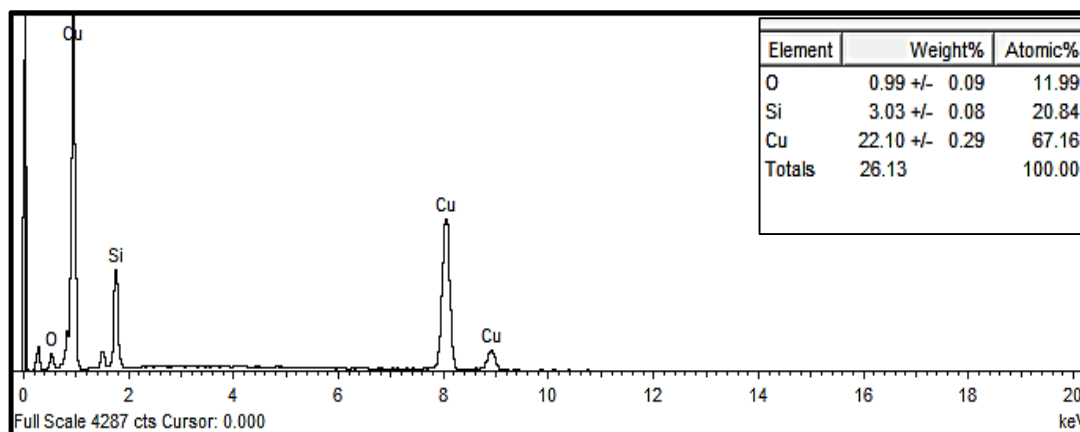

Element	Weight%	Atomic%
O	0.99 +/- 0.09	11.99
Si	3.03 +/- 0.08	20.84
Cu	22.10 +/- 0.29	67.16
Totals	26.13	100.00

Figure 2.2.1 (b) EDS of the as-prepared Si/Cu electrode.

Figure 2.2.1 (c)-(h) show the charge-discharge data for the cell in the operating voltage range 1.2 V to 0.05 V. Fig. 2.2.1(c) shows the cyclability of the Si/Cu electrode for 150 cycles. (d), (e) are the charge-discharge voltage profiles during first cycle, second cycle, and (f) for 10th, 50th, 100th, 150th cycles respectively. The sample shows very high initial discharge capacity

that is close to the theoretical capacity of Si (~3300 mAh/g). The first discharge voltage profile of the sample has a capacity contribution at voltages ~2 V (much higher than 1 V, which could be due to SEI), which could indicate some kind of irreversible redox reaction with the surface.[17] Below 1 V SEI is formed. It is expected that the dominant contribution to capacity is derived from the alloying reaction between Li and Si that generally occurs at potentials of ≤0.2 V.[30] From the second cycle onwards, these feathers of electrolyte decomposition products or side reactions are not observed. We have limited the cut-off voltages till 0.05 V in order to reduce pulverization and get good cycle life.
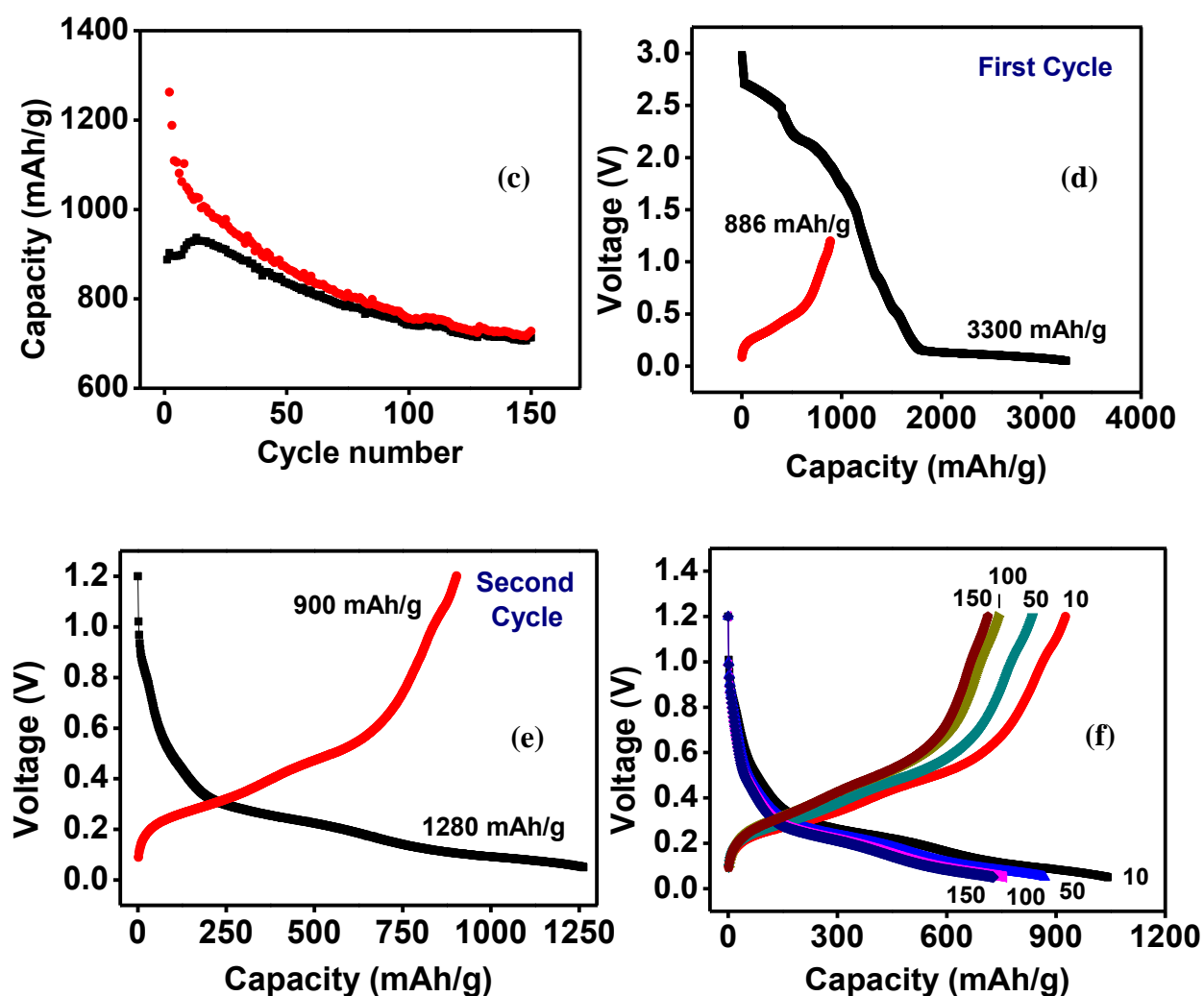

Figure 2.2.1 (c) Cycle-life data for Si/Cu electrode of 150 cycles in voltage range 1.2 V to 0.05 V; voltage profiles for **(d)** first cycle; **(e)** second cycle; **(f)** 10th, 50th, 100th and 150th cycles for Si/Cu electrode in the voltage range of 1.2 to 0.05 V.

From the voltage profiles, it is seen that the Si/Cu electrode that was cycled in the voltage window of 1.2 – 0.05 V retained more than 850 mAh/g capacity after 50 cycles, and more than 700 mAh/g capacity after 150 cycles at C/10 rate, with high Coulombic efficiency (> 90% after the 10th cycle, 96-98% beyond the 50th cycle).

The dQ/dV vs. Voltage plot for the Si/Cu electrode is shown in Fig. 2.2.1 (g). It is reported that after the first cycle, crystalline Si transforms to amorphous silicon.[31] The peaks corresponding to positive values of differential capacity represent delithiation (charge) while those corresponding to negative differential capacity arise due to lithiation (discharge). These peaks may be ascribed to reaction of Li with amorphous Si, and different phase transitions between crystalline and amorphous Li_xSi phases.
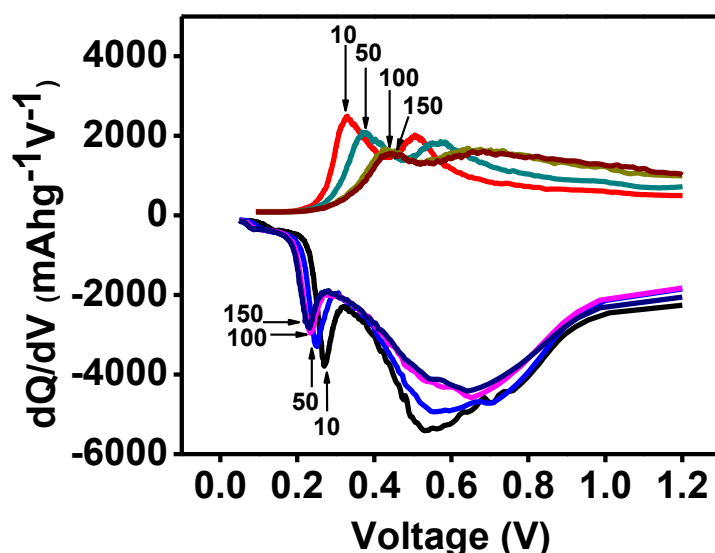

Figure 2.2.1 (g) Differential capacity plot for the Si/Cu electrode.

The rate capability studies performed at C/10, C/7, C/5, C/2 and 1 C rates, is shown in Figure 2.2.1 (h). The Si/Cu electrode shows excellent rate capability. More than 530 mAh/g capacity is retained even after 250 cycles, and more than 500 mAh/g specific capacity is obtained even after 350 cycles, at 1 C rate.
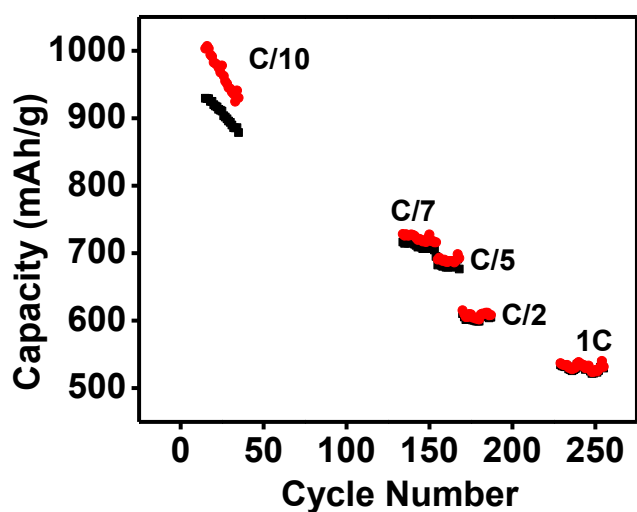
Figure 2.2.1 (h) C-Rate studies for the Si/Cu electrode in the voltage range between 1.2 V and 0.05 V.

Figure 2.2.1 (i) shows the Nyquist plot for the as-prepared Si/Cu electrode, both before and after cycling. The solution resistance or Ohmic resistance (R_Ω) is seen to be as low as 2.6 Ω. The cell impedance in the delithiated state (1.2 V) does not show appreciable change from that in the lithiated state (0.1 V). Moreover, the impedance of the cell after 300 cycles shows very little change in transfer resistance (R_{CT} before cycling = 250 Ω cm^2, R_{CT} after 300 cycles = 450 Ω cm^2) which signifies its excellent electrochemical performance during long cycling.
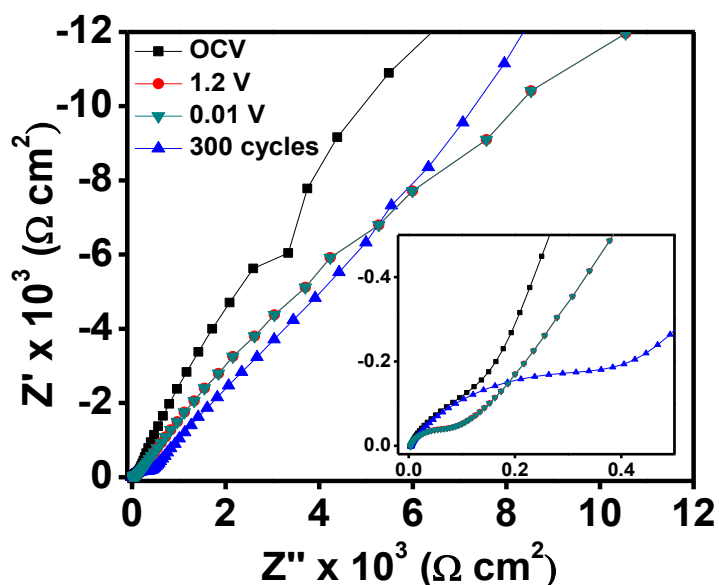

Figure 2.2.1 (i) Nyquist plot for the Si/Cu electrode in the frequency range between 1 MHz and 10 mHz.

The extent of pulverization has been studied at low cut-off voltages by charge-discharge cycling. The voltage profile of the Si/Cu electrode within the operating voltage range 1.2 to 0.01 V is shown in Figure 2.2.1 (j)-(k).
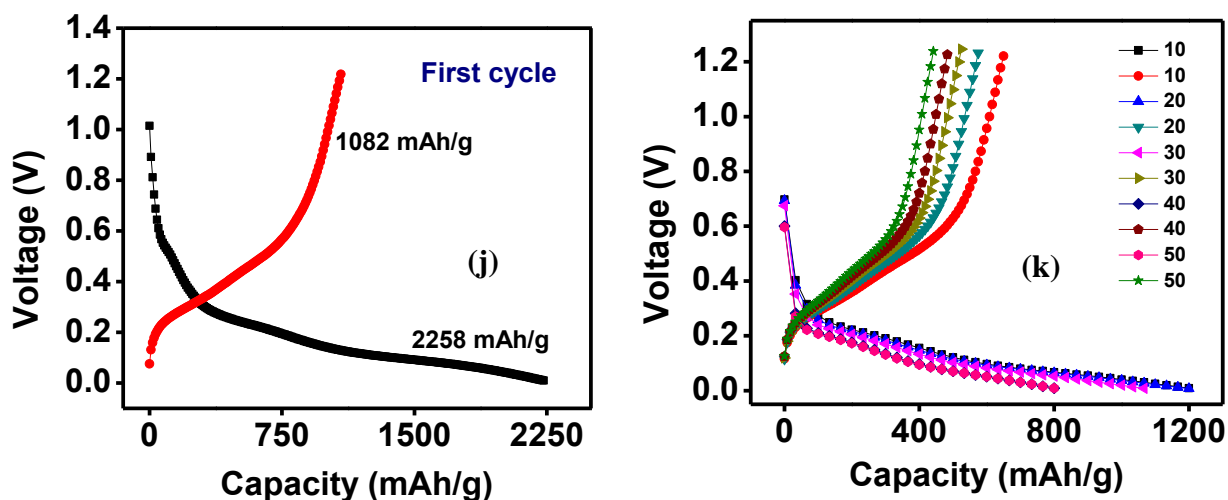

Figure 2.2.1 Voltage profile for **(j)** first cycle; **(k)** 10th, 20th, 30th, 40th and 50th cycles for the Si/Cu electrode between 1.2 and 0.01 V.

As compared to the Si/Cu electrode cycled in the voltage window 1.2 - 0.05 V, the electrode cycled in the 1.2 V - 0.01 V range shows slightly better initial capacities and much lower Coulombic efficiency. The capacity decay is faster during cycling, suggesting that the extent of pulverization has increased with depth of discharge.

Besides the true capacity estimation of Silicon, the electrochemical performance of real electrodes (with binder and conductive diluents) prepared by slurry method is given in Figure 2.2.1 (l)-(o). The electrode prepared by slurry approach showed a rapid capacity fade (Figure 2.2.1 (l)). While first discharge capacity is close to the theoretical capacity (within limits of experimental error), it decays to as low as 85 mAh/g capacity by the 10th cycle (Figure 2.2.1 (m), (o)). The failure of the cell may be attributed to the pulverization that takes place when Si is coated on Cu foil with PVDF as binder. It is likely that this conventional approach may involve a certain degree of agglomeration of particles, and the absence of sufficient spaces between these particles causes them to fracture and detach from the current collector. Moreover, it is possible that in presence of the organic binder, a resistive layer tends to exist

between the current collector and the silicon active material, preventing the proper adhesion of the latter and consequently interfering in electron transport.
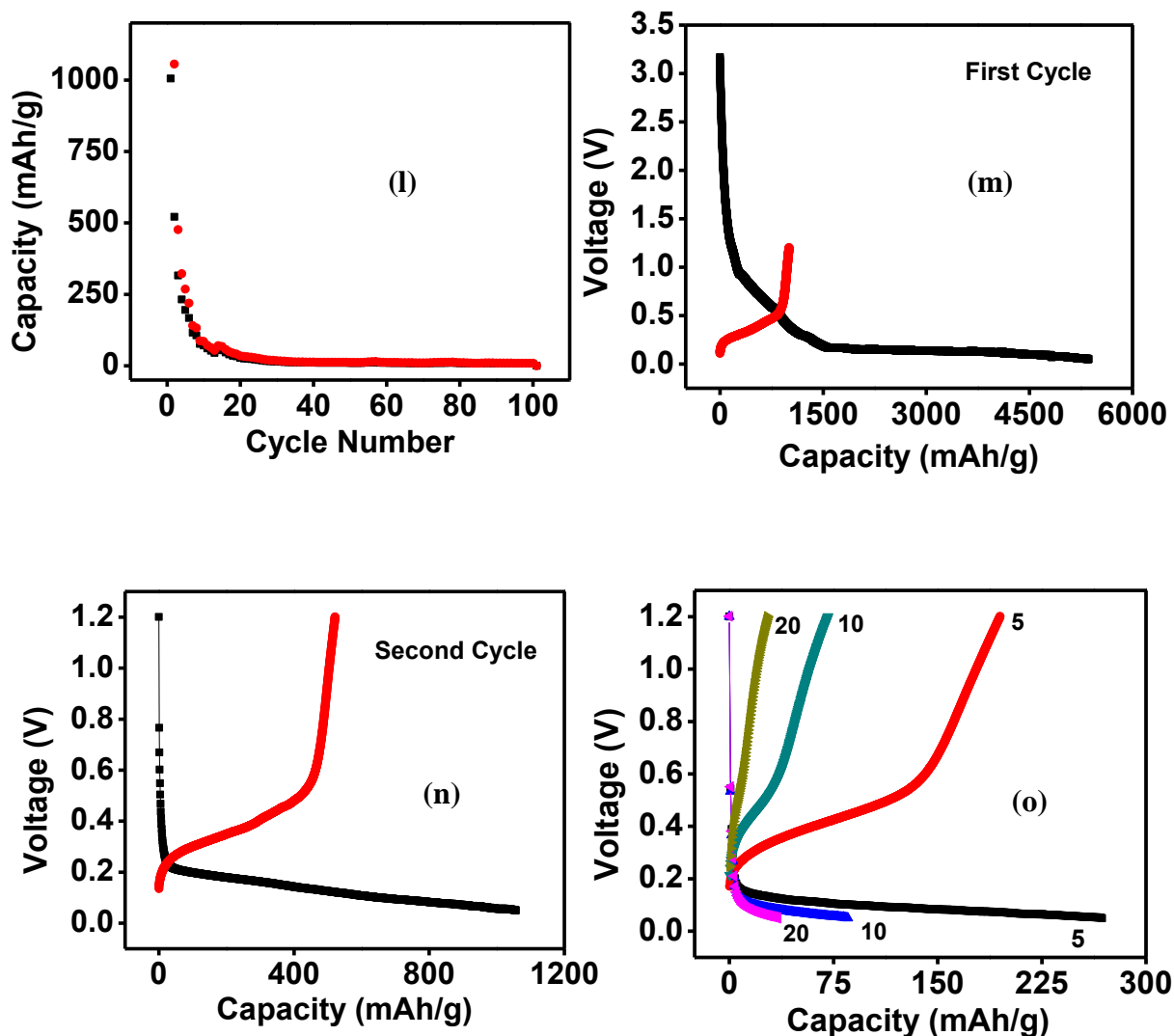

Figure 2.2.1 (l) Cyclability of 100 cycles; voltage profiles for **(m)** first cycle; **(n)** second cycle; **(o)** 5th, 10th and 20th cycles of electrode prepared by slurry method.

In any electrode, the cohesive forces between the binder and the active material play an important role. While some binders may be better suited to a specific active material than others, the binder itself may be responsible for lowering the capacity. Firstly, the electrochemically inactive binder itself may contribute to the impedance of the cell and

secondly, the resistive layer of micro or nano dimensions that tends to exist between the active material and the current collector in spite of the use of an organic binder tends to interfere with the electron transport, resulting in poor electrochemical performance.

The as-prepared Si/Cu electrode tackles the challenge of silicon anodes in multifaceted ways. In this approach, we have not used any conductive additive or any additional binder. Consequently, the entire electrode material is electrochemically active, and contributes to the capacity of the cell. The silicon has been embedded onto the copper foil by the application of pressure. This ensures excellent adhesion of the active material to the current collector, without leaving any space for a resistive layer that would else have interfered with the electron transport. Moreover, electrodes with less silicon content have been shown to cycle at larger capcities.[32] In our Si/Cu electrode, the silicon content is about 20% (as seen from EDS studies) and the particles are distributed irregularly on the copper foil with sufficient gaps between them, thus providing enough space to accommodate the volume expansion and compression of the silicon nanoparticles. This accounts for the reasonably high capacity and remarkably stable cycling of the electrode.

2.2.2 3D Electrode architecture for Lithium Ion Batteries with different binders

Objective: The absence of carbon black was seen to lower the real capacity of Si NPs, possibly due to reduced conductivity and loss of electrical contact to some extent. Our approach was to increase the conductivity by using 3D electrode architecture of carbon fibre (CF) mats as current collector.

Carbon fibers (CFs) are of interest in energy storage applications as they possess a range of useful properties, including high electronic and thermal conductivities, chemical stability and corrosion resistance.[33,34] This, coupled with the high-voltage stability of CFs, makes them an attractive choice as current collector for the development of advanced lithium ion batteries with alternative architectures.

Approach: Cu foil was replaced with carbon fibre mats as current collector. In doing so, the active material no longer forms a surface coating (as on Cu current collector), but gets embedded between and along the fibres, giving rise to a three-dimensional electrode structure which results in reduced pulverization and enhanced conductivity. This approach is suitably explained in Figure 2.2.2.
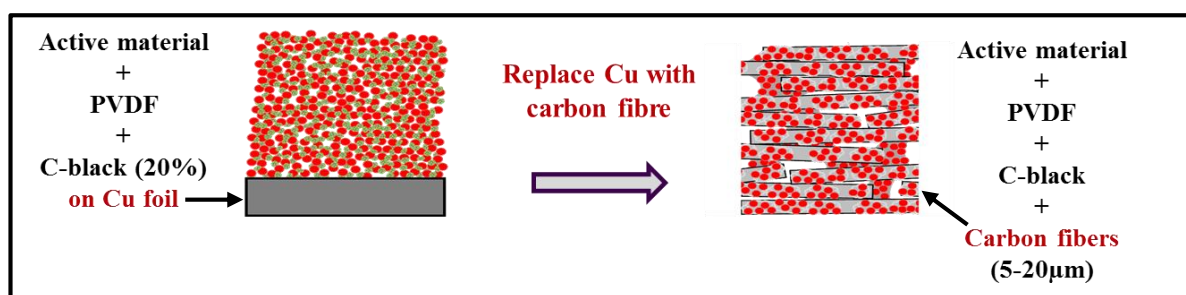

Figure 2.2.2 Approach to 3D Electrode architecture.

Based on the 3D electrode architecture approach, four types of cells were fabricated. In all cases, carbon fibre was used as the current collector. Modifications were made at each step in an attempt to enhance the electrochemical performance, either by incorporating additional carbon additives to increase the conductivity or by using novel binders to replace the conventional polymeric organic binder.

2.2.2.1 Silicon NPs coated on carbon fibre using PVDF as binder

2.2.2.1(a) Experimental: The electrode was fabricated by mixing the active material (Si NPs, 82 wt%), carbon black (10 wt%) and binder (8 wt% PVDF, dissolved in NMP) to form a slurry. The slurry was then coated onto carbon fibre, and dried at 80 ℃ on a hot plate followed by punching to 1 cm^2 size electrode. The as-prepared electrode was characterized using X-ray diffraction and Swagelok-type cells were assembled in the glove box using lithium foil counter electrode for electrochemical measurements as discussed in Section 2.2.1(a).

2.2.2.1(b) Result and discussion: The X-Ray diffraction pattern shows the characteristic peaks for silicon, as seen in Fig. 2.2.2.1(a). The characteristic broad peak for carbon fibre is also observed. This confirms the coating of Si onto CF.
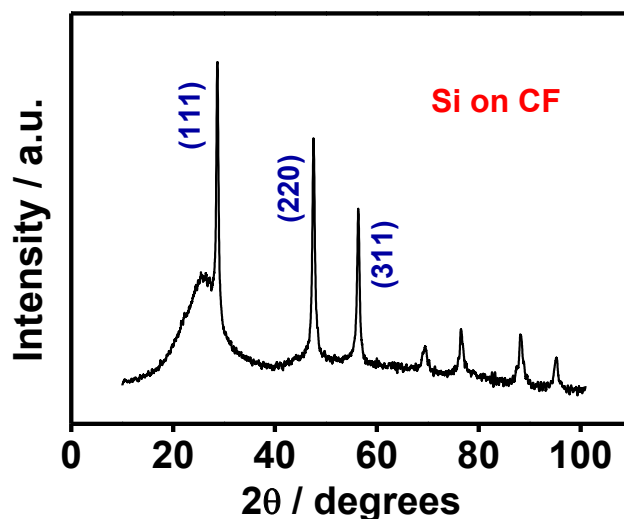

Figure 2.2.2.1 (a) X-Ray Diffraction pattern for the as-prepared Silicon composite electrode.

Figure 2.2.2.1 (b)-(d) show the cyclability and the galvanostatic charge-discharge profiles for the as-prepared electrodes.
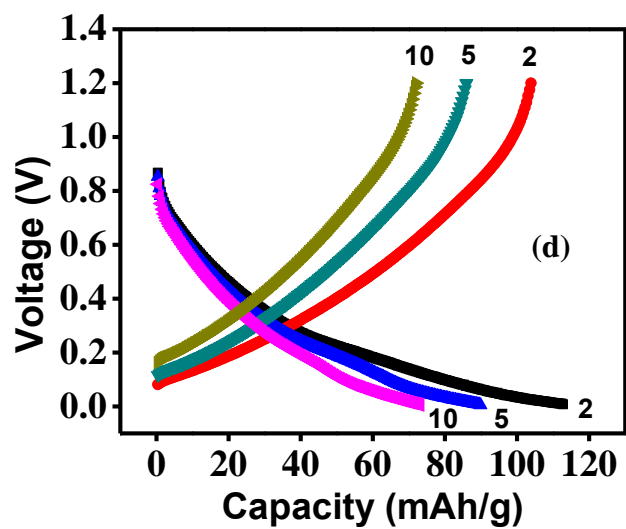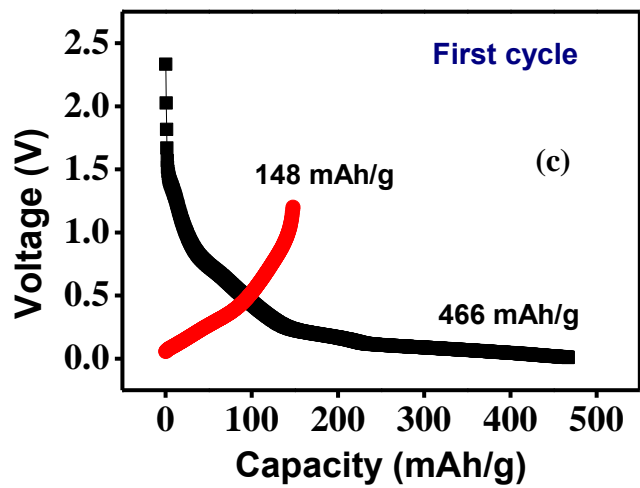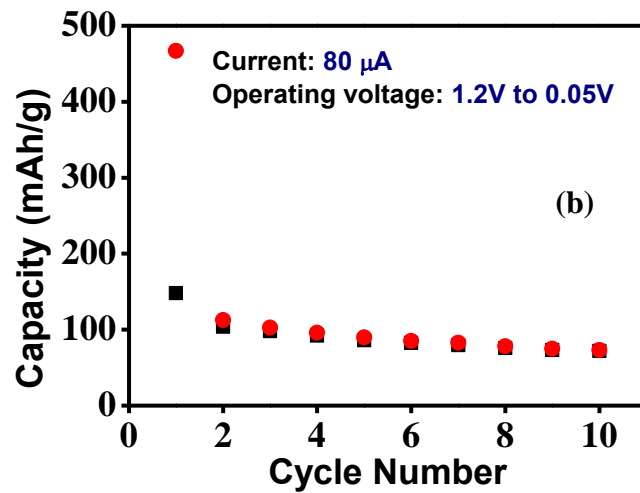
Figure 2.2.2.1 (b) Cyclability of 10 cycles; galvanostatic voltage profile of **(c)** first cycle, **(d)** second, fifth and tenth cycles, for the as-prepared electrode.

From the voltage profiles and cycle life data (Figure 2.2.2.1(b)-(d)), first lithiation and delithiation capacities were observed to be 466 mAh/g and 148 mAh/g, respectively. Upon cycling, rapid capacity fade was observed. This may be due to the resisitivity of the PVDF binder. It is likely that the binder does not allow the active material to attach well to the carbon fibre, as a result of which pulverization takes place, causing loss of capacity. Besides, the capacity could be due to carbon fiber alone not due to silicon.

2.2.2.2 Silicon NPs + CNT coated on carbon fibre using PVDF as binder

Rapid capacity fading was observed when Si NPS were coated on carbon fibre using PVDF as binder. In our second method, we used same approach as given in 2.2.2.1, i,e., carbon fibre as the current collector, carbon black as conductive additive and PVDF as binder, but carbon nanotubes (CNTs) (10 %) was used as an additive to the active material to enhance conductivity further. There are mainly two features that make CNTs interesting for Li-ion battery applications. Firstly, their high electronic conductivity as compared to carbon blacks makes them a better conductive additive and secondly, their ability to insert Li ions allows them to be used as an active material for anodes.

2.2.2.2(a) Experimental: A mixture of Silicon NPs (90 wt%) and CNTs (10 wt%) were ball-milled for 12 hours. Slurry was prepared containing the ball-milled Si-CNT mixture (82 wt%), C-black (10 wt%) and PVDF (8 wt%, dissolved in NMP) and coated on carbon fibre, which was dried at 80 ℃. The as-prepared electrode was characterized using X-Ray Diffraction and its electrochemical performance as an anode was tested in a Swagelok-type cells as detailed in Section 2.2.1(a). Galvanostatic charge-discharge cycling was conducted in the potential range between 1.2 V and 0.005 V.

2.2.2.2(b) Results and discussion: The XRD Pattern in Figure 2.2.2.2 (a) shows characteristic Si peaks .
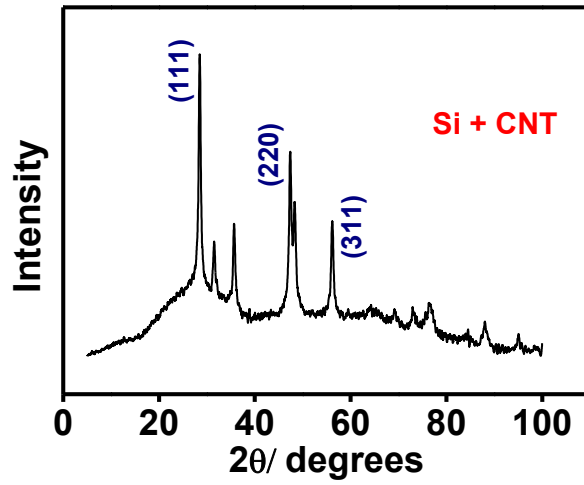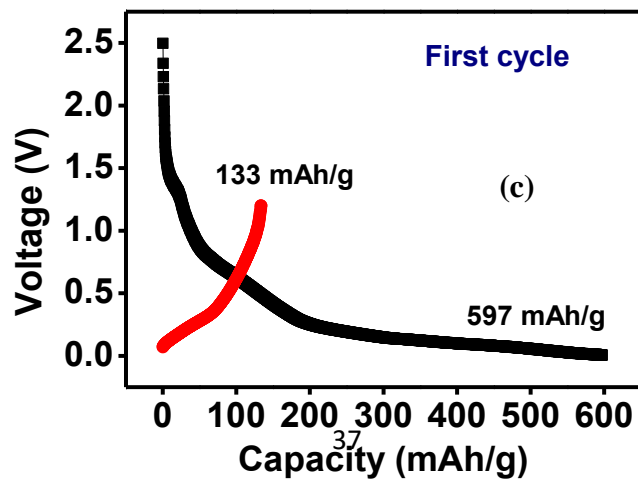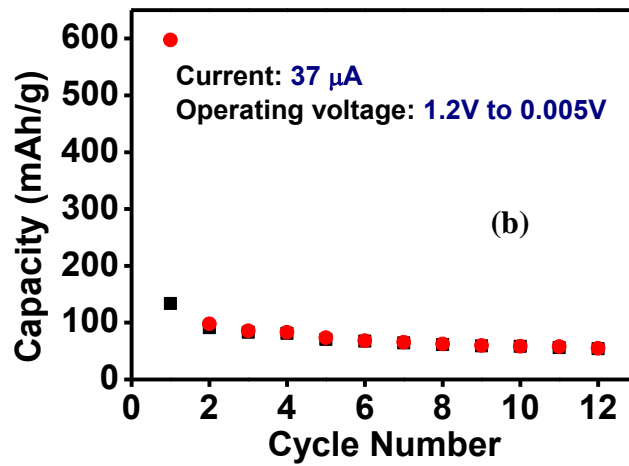
Figure 2.2.2.2 (a) X-Ray Diffraction pattern of the as-prepared electrode Si-C-CNT mixed composite electrode.

The charge-discharge profile (Figure 2.2.2.2 (b)-(d)) was similar to the previous approach (Section 2.2.2.1).
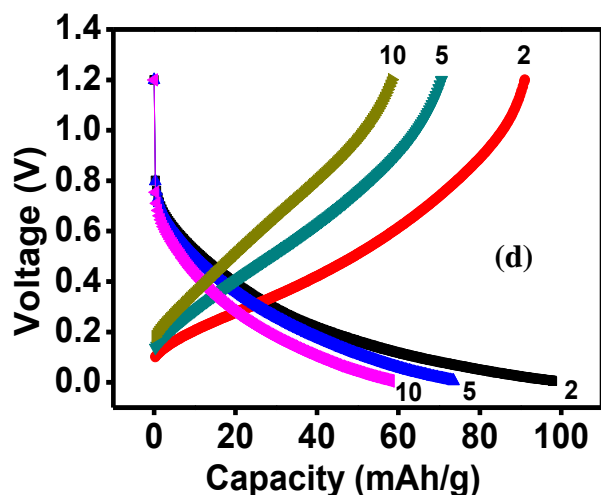
Figure 2.2.2.2 (b) Cyclability of 12 cycles; galvanostatic voltage profile of **(c)** first cycle, **(d)** second, fifth and tenth cycles.

The addition of CNT did not improve the electrochemical performance of silicon. Rapid capacity fading was observed (Figure 2.2.2.2 (b)-(d)), possibly due to the resistivity of the binder and improper attachment of the Si NPs to the current collector, resulting in pulverization.

2.2.2.3 Silicon NPs coated on carbon fibre using chitosan as binder

Chitin, poly (β-(1→4)-*n*-acetyl-d-glucosamine), is a linear natural polysachharide of major importance, obtained from the exoskeleton of marine crustaceans. Partial deacetylation of chitin under alkaline conditions gives chitosan, which is the most important chitin derivative in terms of applications.[35]
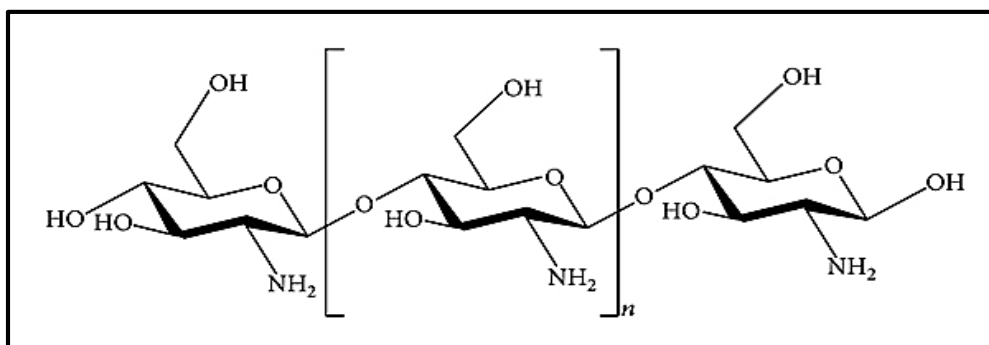
Figure 2.2.2.3.1 Structure of chitosan.

Chitosan is a naturally abundant, renewable polymer having excellent properties such as biodegradability, bio-compatibility and non-toxicity.[36] Chitosan-based aqueous slurry possesses good viscosity, which can be considered as an effective electrode binder. This was first shown in the work by Zheng et al. in 2013, wherein an acid solution-based chitosan slurry was applied as the binder for a commercial spherical graphite material.[37] Their results showed that the graphite anode employing chitosan exhibited enhanced electrochemical performances in terms of the first columbic efficiency, rate capability and cycling behaviour, as compared to that using the conventional PVDF binder. In 2014, carboxymethyl chitosan (C-chitosan) was investigated as a water soluble binder for silicon anodes by Zhang et al [38], thus paving the way for subsequent research on a series of novel binders from the chitosan family. In both the mentioned cases, Cu foil was used as the current collector.

In our approach, to overcome the problems of pulverization, binding property with chitosan as a binder has been explored.

2.2.2.3(a) Experimental: Chitosan was dissolved in 0.5 wt% acetic acid solution to a concentration of 3 wt%. The dispersion was stirred magnetically for 2 hours at room temperature. A slurry was prepared containing 84 wt% Si NPs, 10 wt% carbon black and 6 wt% of the chitosan solution, and stirred for 5 hours. The slurry was then coated on a piece of carbon fibre which was dried overnight, and used as an anode in a Swagelok-type cell which was assembled as described in Section 2.2.1(a). Galvanostatic charge-discharge cycling was carried out in the voltage windows of 1.2 - 0.005 V.

2.2.2.3(b) Results and discussion: The charge-discharge cycle life and voltage profiles for the as-prepared electrodes are shown in Figure 2.2.2.3 (a)-(c). The electrochemical performance was seen to be very poor—the cell did not work at all.
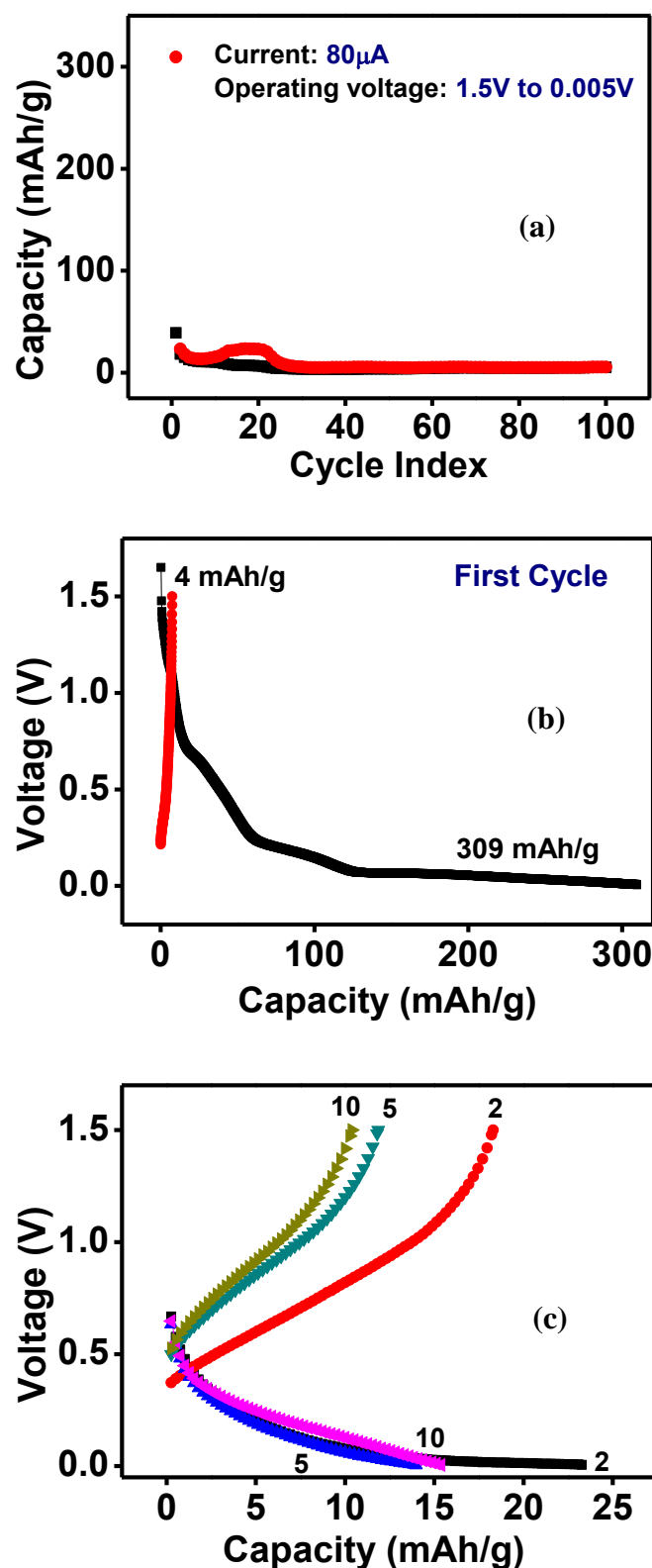
Figure 2.2.2.3.2 (a) Cycle life data; galvanostatic charge-discharge voltage profile of **(b)** first cycle, **(c)** second, fifth and tenth cycles of Silicon NPs coated on carbon fibre using chitosan as binder.

The failure of the cell is possibly due to the inability of chitosan to act as a conductive, binding matrix that would hold the active material to the carbon fibre. The presence of an additional conductive additive, such as carbon, might have ensured better electrochemical performance.

2.2.2.4 Si NPs coated on carbon fibre using hydrogel as binder

A hydrogel is a network of polymer chains that are hydrophilic, sometimes found as a colloidal gel in which water is the dispersion medium. They are synthesized from hydrophilic monomers by either chain or step growth, along with a functional cross linker to promote network formation.

The three-dimensional networks of hydrogels can swell in water and aqueous solutions.[39] This reversible swelling-deswelling property also allows them to retain a large volume of liquid in the swollen state. The equilibrium swelling degree and elastic modulus of hydrogels depend on the cross-link, charge densities of the polymer network and also on the cross-linked polymer concentration after gel preparation.[40] Hydrogels can thus be designed to perform dramatic volume transition in response to a variety of physical and chemical stimuli. It has also been shown that hydrogels can be made electrically conductive by embedding various conducting components (e.g., carbon, conducting polymers and metal nanomaterials) into aqueous gels[41], a property which is widely exploited in making biosensors.

Since they can absorb large quantities of biological fluids, hydrogels have a wide range of applications in biomedical and biological fields. They are also used as capacitors as electrode materials and in the form of membrane electrolytes as they boost capacitive performance. In addition, hydrogels find use in paints, cosmetics, jellies and numerous other applications in our daily lives.

Due to their interesting properties, hydrogels have been used as binders in different battery systems. For instance, agar chemical hydrogel (ACH) binders have been reported for fuel-

electrolyte-fed fuel cells[42], and chitosan chemical hydrogel (CCH) has proved to be a novel, cost-effective binder for direct borohydride fuel cells (DBFC) [43]. They find use in stabilising the structure of other materials, as in lithium ion batteries, where they may help in mitigating problems arising due to volume modifications. For example, an Alginate hydrogel binder prepared through the cross linking effect of Sodium Alginate with Ca^{2+} ions, has been shown to enhance the electrochemical performance of a Si/C anode of a Li-ion battery, wherein the hydrogel has been found beneficial in maintaining the electrode structure without pulverization.[44] Similar work is also known on Si-PANI hydrogel[45] and Si-PAA/PANI composite hydrogels[46].

In our approach, we prepared a conductive, elastic polypyrrole hydrogel using $Fe(NO_3)_3.9H_2O$ as the oxidant, following the procedure adopted by Lu, He at al.[41] Our goal was to synthesize the hydrogel as an elastic, conducting matrix around the Si nanoparticles such that the Si NPs will remain embedded within the hydrogel, even if they get disconnected from the current collector due to volume modification. This will help alleviate the problem of pulverization, allowing for stable cycling.

2.2.2.4(a) Experimental: Pyrrole (0.866 ml, 12.52 mmol) was dissolved in 6 ml H_2O/EtOH (v/v 1:1) to form a colourless solution. 80 mg of silicon nanoparticles was added to the pyrrole solution, and stirred for about 15 minutes. A preweighed piece of carbon fibre was added to the suspension, and the slurry was stirred for about 30 min. In another beaker, 5.06 g (12.52 mmol) of $Fe(NO_3)_3.9H_2O$ was dissolved in 6.0 ml H_2O/EtOH (v/v 1:1), and this solution was added to the pyrrole-silicon slurry under vigorous agitation at 0-4 ºC. The mixture was stirred for 30 seconds before standing, and formed gel in several minutes. The carbon fibre was retrieved from the gel, dried overnight, washed repeatedly in H_2O/EtOH (v/v 1:1) mixture to remove the ferric nitrate and then dried again. The as-prepared Si/PPy-hydrogel electrode on carbon fibre was then characterised using X-Ray diffraction and used as anode in a Swagelok type cell which whose electrochemical performance was tested as detailed in Section 2.2.1(a).

2.2.2.4(b) Results and Discussion: The X-Ray Diffraction pattern of the as-prepared Si/PPy hydrogel electrode is shown in Fig. 2.2.2.4(a). All characteristic peaks for Si are observed, along with a broad hump around 28º due to the carbon fibre current collector. Initial broad peak is due to polypyrrole.
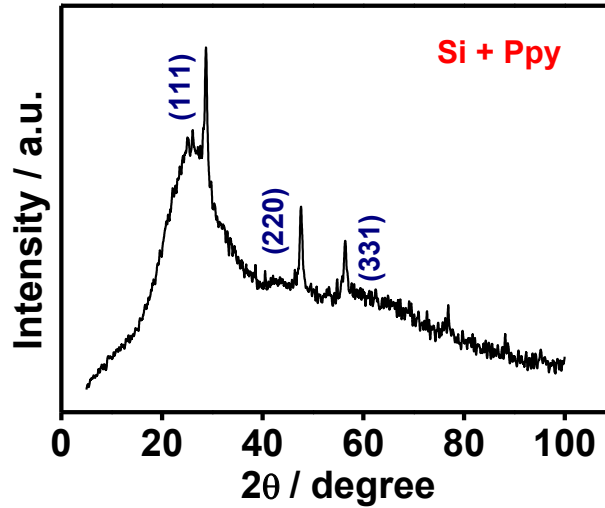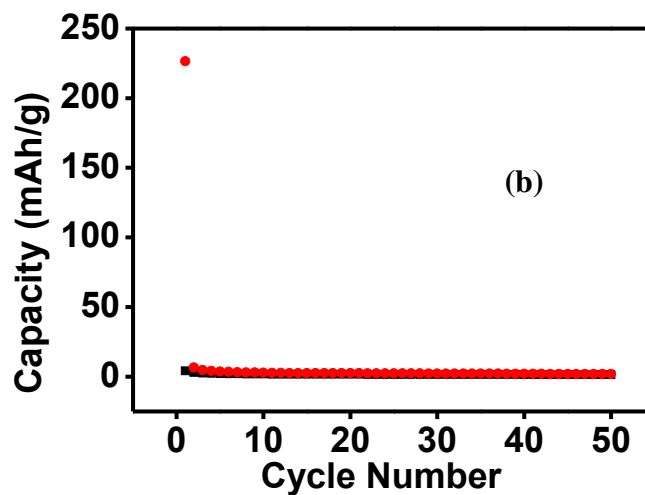

Figure 2.2.2.4 (a) X-Ray Diffraction Pattern of the as-prepared electrode.

Cycle life and galvanostatic charge-discharge data presented in Figure 2.2.2.4 (b)-(d) clearly indicate that the Si/PPy hydrogel electrode too failed to work.
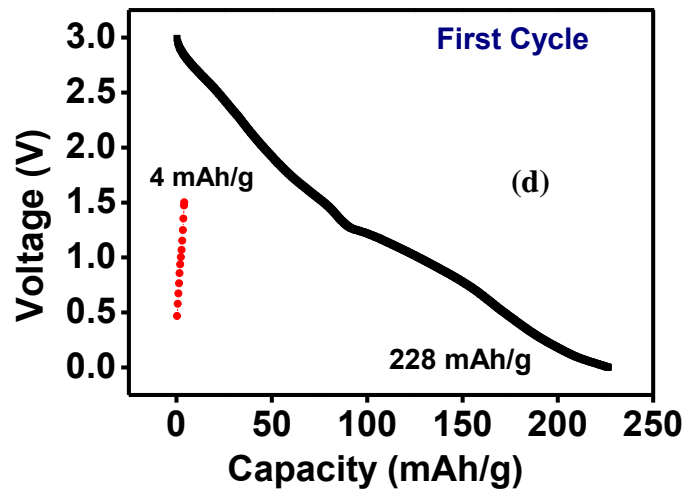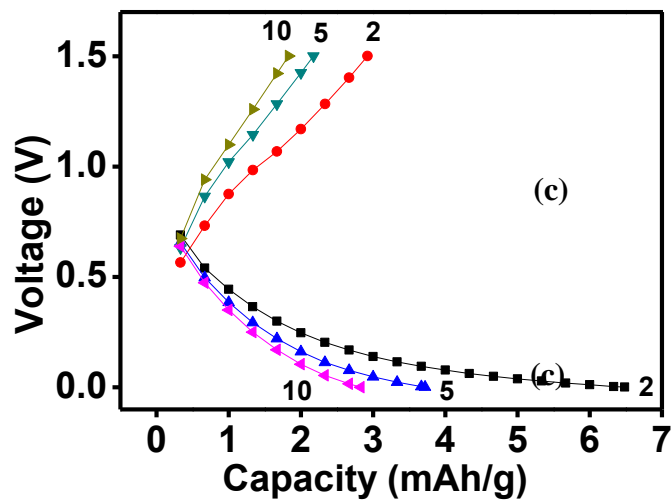
Figure 2.2.2.4 (b) Cycle life data for 50 cycles; galvanostatic charge-discharge voltage profiles of **(c)** first cycle and **(d)** second, fifth and tenth cycle for Si NPs coated on carbon fibre using hydrogel as binder.

The failure of the cell is possibly due to the absence of any conductive additive and also the inability of the hydrogel to form an elastic matrix around the Si NPs. The latter might owe its cause to the lack of a sufficiently long curing process, during which the hydrogel would have undergone secondary microstructural changes that would, in turn, have enhanced its elasticity and swelling-deswelling properties.

2.3 High temperature carbon binder electrode architecture for Silicon anodes

As an alternative to using inactive polymeric binders, carbon fibre mats may be coated with a suitable carbon source that can ensure good adhesion between the current collector and active material. This approach eliminates the need for organic binders (PVDF) or metal current collectors (Cu foil), thereby increasing the energy density of the battery. Because of the high temperature properties of the CFs, it is possible to form strong, conductive bonds with mesophase pitch as the carbon precursor.[47]

Research has shown that petroleum pitch (P-Pitch) coated carbon fibre mats can replace Al foil as the current collector in lithium ion batteries.[33] CFs coated with slurry of pitch and active material in N-vinyl-2-pyrrolidone (NVP) are annealed at high temperature of 500-1000 $^{\circ}$C under argon to carbonize the pitch, which then forms a uniform coating along the fibres and ensures robust adhesion of the active mass to the current collector. This electrode fabrication technique has been applied to cathode materials such as LiFePO$_4$, where prolonged cycling >200 cycles has been demonstrated with relatively low capacity fading.

In our work, we have applied the aforementioned approach to Silicon anodes by using P-Pitch as a high temperature carbon binder and carbon fibre as the current collector. This may be schematically depicted as follows:
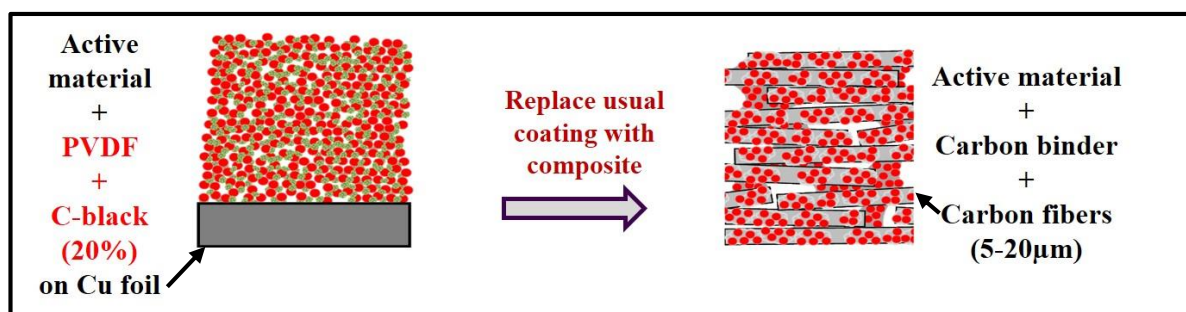

Figure 2.3.1 Approach to 3D Electrode architecture using a carbon binder.

2.3(a) Experimental: A slurry of P-Pitch (50 wt%) and Si NPs (50 wt%) was prepared in NVP by thorough mixing on a vortex mixture. The carbon fibre was coated with the as-prepared slurry. The excess slurry was then carefully removed from the surface of the CF, followed by drying at 90 ºC. The sheets were then calendared, followed by heating at 900 ºC under Argon atmosphere for 5 hours to carbonize the petroleum pitch. The as-prepared electrode was characterized using X-Ray Diffraction, Scanning Electron Microscopy and Raman Spectroscopy. The carbon coating of Si NPs was also observed by Transmission Electron Microscopy. This electrode was used as the anode in a Swagelok type cell, which was fabricated as described in Section 2.2.1(a). Galvanostatic charge-discharge was carried out between 1.2 V and 0.05 V. The carbon precursor (petroleum pitch) and the current collector (carbon fibre) were also structurally characterized using SEM and Raman Spectroscopy.

2.3(b) Results and Discussion: The structural characterizations of the precursors are presented in Figure 2.3.2 (a)-(d). (a) and (b) show the SEM image and Raman spectrum, respectively, of the CF. From the SEM image, the diameter of the individual fibres is seen to ~5 μm. The Raman spectrum shows the D-band (Defect or Disorder band) and G-band (Graphitic band) which are characteristic of sp^2 hybridised carbon systems. The D-mode is caused by the disordered structure of grapheme, while the G-band arises from the stretching of the C-C bond in graphitic materials, and is common to all sp^2 carbon systems. (c) and (d) show the SEM image and Raman spectrum, repetively, of carbonized P-Pitch. The vacant space available within the matrix of carbonized Pitch is evident from the SEM image. The Raman spectrum shows the characteristic D and G bands, as mentioned previously.
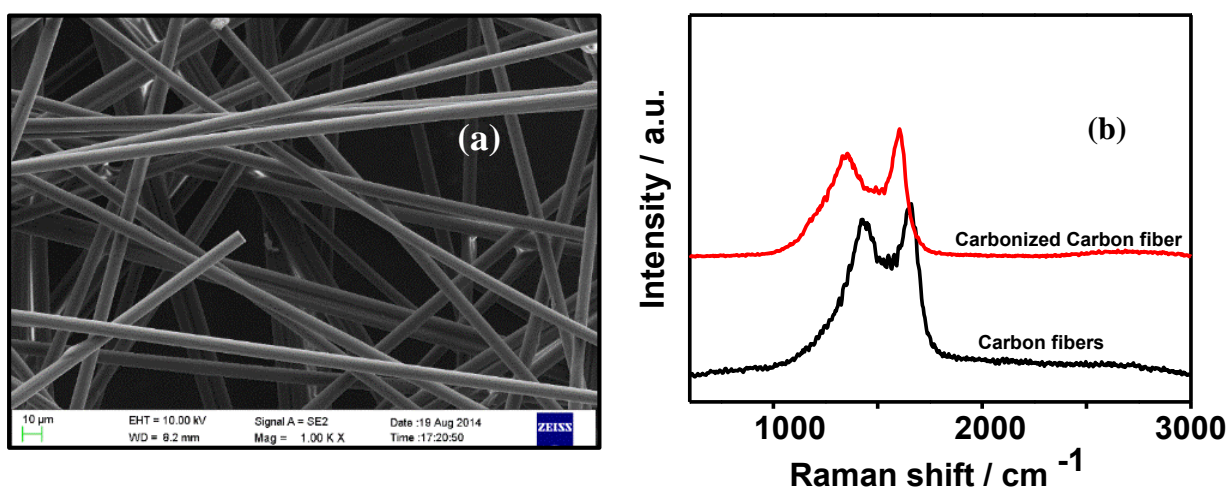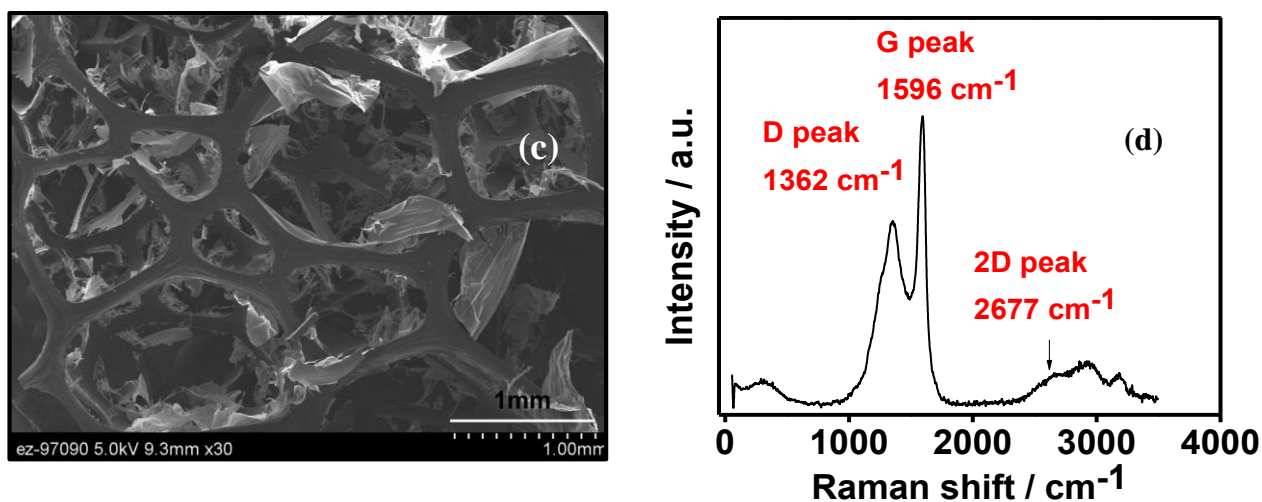
Figure 2.3.2 SEM image and **(b)** Raman spectra of carbon fibre; **(c)** SEM image and **(d)** Raman spectra of carbonized P-Pitch at 900 ℃.

The structural characterization for the electrode prepared with P-Pitch as a high temperature carbon binder is presented in Figure 2.3.3. Figure 2.3.3 (a), (b) and (c) show the SEM image, Raman spectrum and X-Ray Diffraction pattern of the as-prepared Si-C composite electrode on CF, respectively. The SEM image shows the coating of the active material along and between the fibres of the carbon fabric, thus displaying the excellent adhesion of the active material to the current collector. The Raman spectrum shows the major Si-Si stretch at ~510 cm^{-1}, as well as the D and G bands characteristic of the graphitic CF. The XRD pattern shows the characteristic peak for crystalline Si at ~28°, preceded by a hump characteristic of carbon
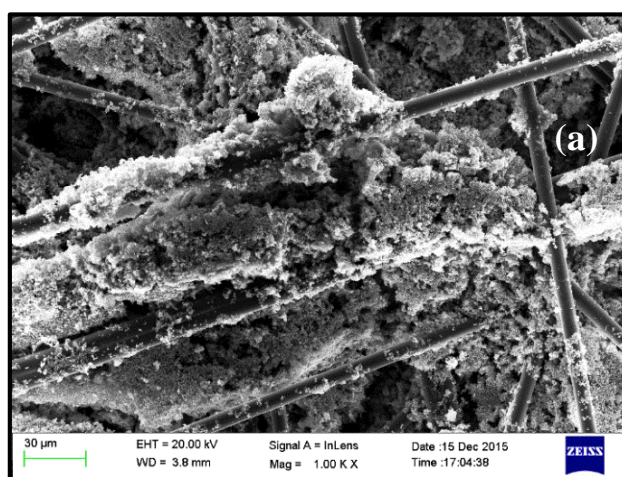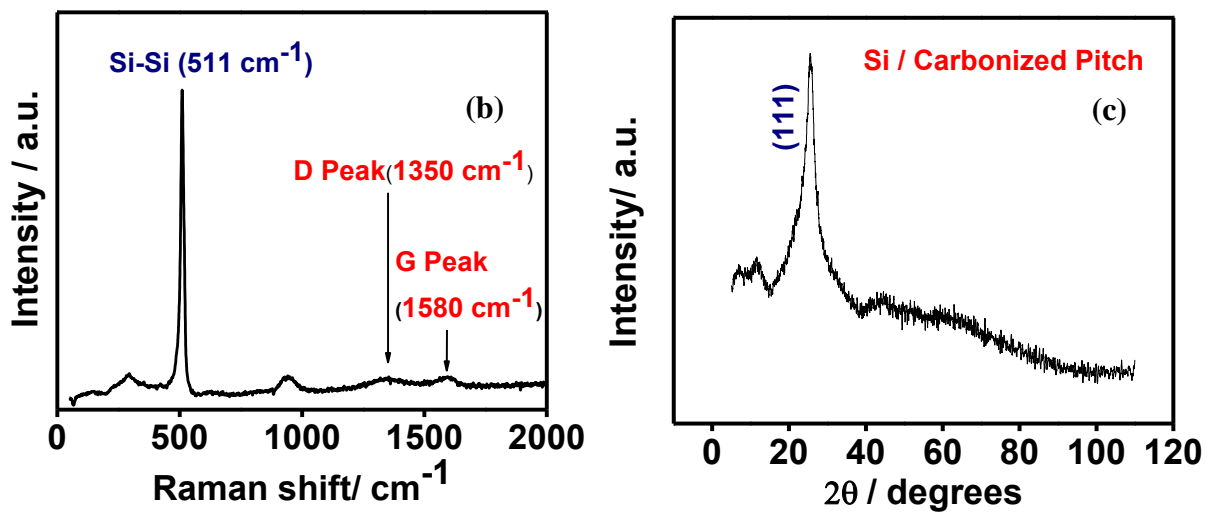
Figure 2.3.3 (a) SEM image; **(b)** Raman shift in cm^{-1}; and **(c)** XRD Pattern of the as-prepared Si/Carbonized-Pitch electrode.

The galvanostatic voltage profile for the as-prepared electrode is given in Figure 2.3.4. The galvanostatic charge-discharge profile clearly indicates that SEI is formed below 0.75 V during the first cycle, similar to silicon electrodes. An initial lithiation capacity of >3500 mAh/g and delithiation capacity of ~ 1800 mAh/g have been achieved in the first cycle.

Figure 2.3.4 Galvanostatic voltage profile of the as-prepared Si/Carbonized Pitch electrode.

The excellent performance of Si-C composite electrode on 3D carbon fiber is due to the fact that P-Pitch, on carbonizing, forms a foam which ensures excellent adhesion of the active material to the carbon fibre and also acts as a matrix with vacant spaces wherein the volume expansion of Si can b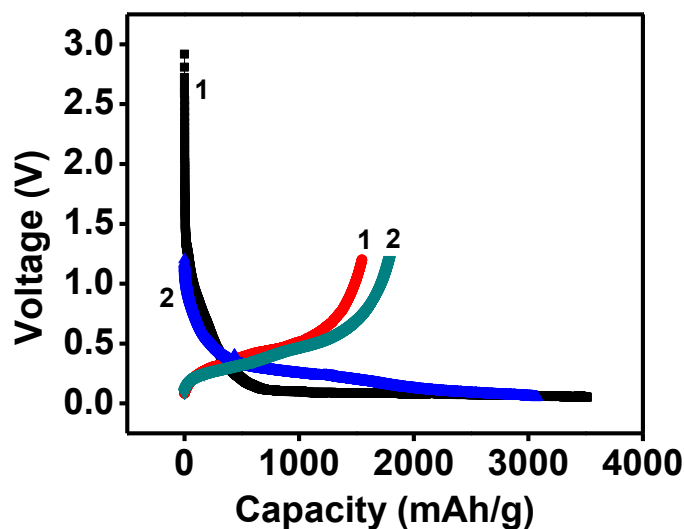e accommodated. This is responsible for the high specific capacities, which are close to the theoretical capacity. This approach has the potential to improve electrochemical performance and also increase the specific energy density of the electrode, since no additional organic binder or current collector is required. Two cycles have been completed, and further cycling is under progress.

In summary, micro CF mat current collectors can be demonstrated as anodes for lithium batteries. This electrode fabrication uses <10% carbon pitch to bond the active material and current collector at 900 ºC, eliminating the use of organic binders and the copper foil current collector. This may increase the cycle life performance of the electrode and with further improvement, should give high specific and volumetric energy density. The CFs allow excellent electronic conductivity and contact (good adhesion) through P-pitch for the active mass which may also serve as a barrier against detrimental capacity loss. We believe that the cost and performance of CF materials, as well as the methods used to coat fibers with the active cathode materials, will continue to improve and that this study is a major step forward in realizing low-cost lithium ion batteries with high specific energy that could be beneficial for building Li-batteries for EV applications.

Conclusion:

Silicon nanoparticles (Si NPs) were synthesized by reverse micelle route and characterized by various surface techniques such as XRD, SEM, Raman etc. The as-synthesized Si NPs are used as active material in developing binder-free anodes for Lithium Ion Batteries. The Si NPs were embedded onto copper foil by the application of pressure, without employing any binder or conductive additive. The as-prepared electrode was tested as anode in a Swagelok cell against pure lithium foil, and its electrochemical performance was compared to conventional electrodes (slurry prepared with Si NPs, PVDF and conductive carbon black). The binder-free Si/Cu electrode was found to retain more than 850 mAh/g capacity after 50 cycles, and more than 700 mAh/g capacity after 150 cycles at C/10 rate, with high Coulombic efficiency (>90 %). The electrode also showed good rate capability, giving more than 500 mAh/g capacity after 350 cycles when cycled at 1 C rate. The excellent capacity retention and cyclability may be attributed to the excellent adhesion of the Si active material to the Cu foil due to application of pressure, and to the entire electrode material being electrochemically active and thereby contributing to the capacity of the cell. In addition, the less loading of Si ensures sufficient gaps between the particles, thus providing enough vacant spaces to accommodate the volume modification of the Si NPs and thereby reducing pulverization. Pulverization and capacity decay have increased with low cut off voltages of 10 mV. 3D electrode architecture for Si anodes were also employed with carbon fibre as current collector and chitosan, polypyrrole hydrogel and P-Pitch as novel binders. However PVDF, chitosan, polypyrrole hydrogel showed poor capacity of the electrode. The electrode fabricated with carbonized P-Pitch as a high-temperature (900 ºC) binder showed high initial delithiation capacities of ~2000 mAh/g, and further work on the same is under progress.

References:

1. B.A. Boukamp, G.C. Lesh and R.A. Huggins*, J. Electrochem. Soc.*, 1981, **128**, 725–729

2. S. Goriparti, E. Miele, F. D. Angelis, E. D. Fabrizio, R. P. Zaccaria and C. Capiglia, *J. Power Sources*, 2014, **257**, 421-443

3. R.A. Huggins, *J. Power Sources*, 1999, **81**, 13—19

4. W.J. Zhang, *J. Power Sources*, 2011, **196**, 13–24

5. H. Wu and Y. Cui, *Nano Today*, 2012, **7**, 416

6. C. K. Chan, H. Peng, G. Liu, K. McIlwrath, X. F. Zhang, R. A. Huggins and Y. Cui, *Nat. Nanotechnol.* 2008, **3**, 31−35

7. N. Liu, L. Hu, M. T. McDowell, A. Jackson and Y. Cui, *ACS Nano*, 2011, **5**, 6487–6493

8. L.F. Cui, R. Ruffo, C. K. Chan, H. Peng and Y. Cui, *Nano Lett.*, 2009, **9**, 491–495

9. T. Song, J. Xia, J. A. Rogers, U. Paik et al., *Nano Lett.*, 2010, **10**, 1710–1716

10. M.H. Park, M.G. Kim, Y. Cui, J. Cho et al., *Nano Lett.*, 2009, **9**, 3844-3847

11. J. Qua, H. Li, J. J. Henry Jr., S. K. Martha, N. J. Dudney, H. Xua, M. Chi, M. J. Lance, S. M. Mahurin, T. M. Besmann and S. Dai, *J. Power Sources*, 2012*, 198*, *312– 317*

12. Y. Yao, M. T. McDowell, Y. Cui et al., *Nano Lett.*, 2011, **11**, 2949–2954

13. J. P. Maranchi, A. F. Hepp and P. N. Kumta, *Electrochem. Solid State Lett.,* 2003, **6**, A198-A201

14. J. Liang, X. Li, Y. Zhu, Y Qian et al., *Nanoscale*, 2015, **7**, 3440-3444

15. H. Kim, B. Han, J. Choo and J. Cho, *Angew. Chem. Int. Ed.,* 2008, **47**, 10151 –10154

16. X. Zhu, D. Yang, J. Li and F. Su, *J. Nanosci Nanotechnol.* 2015, **15**, 15-30

17. H. Zhou, J. Nanda, S. K. Martha, R. R. Unocic, H. M. Meyer, Y. Sahoo, P. Miskiewicz and T. F. Albrecht, *ACS Appl. Mater. Interfaces*, 2014, **6**, 7607−7614

18. X. Zhao, A.M. Cao, L. Wan and Y.G. Guo, *Nano Res.*, 2012, **5**, 845-853

19. B. Wang, X. Li, B. Luo, Y. Jia and L. Zhi, *Nanoscale*, 2013, **5**, 1470-1474

20. L. F. Cui, L. Hu, J. W. Choi and Y. Cui, *ACS Nano*, 2010, **4**, 3671–3678

21. A. M. Chockla, J. T. Harris, B. A. Korgel et al., *J. Am. Chem. Soc.* 2011, **133**, 20914–20921

22. L. F. Cui, Y. Yang, C. M. Hsu and Y. Cui, *Nano Lett.,* 2009, **9**, 3370–3374

23. H. Yoo, J. I. Lee, H. Kim, J. P. Lee, J. Cho and S. Park, *Nano Lett.,* 2011, **11**, 4324–4328

24. M. Thakur, M. Isaacson, S. L. Sinsabaugh, M. S. Wong and S. L. Biswal*, J. Power Sources,* 2012, **205***,* 426– 432

25. K. Fu , O. Yildiz and P. D. Bradford, *Adv. Mater.,* 2013, **25**, 5109–5114

26. N. Liu, Z. Lu, J. Zhao, M. T. McDowell, H. –W. Lee, W. Zhao and Y. Cui*, Nature Nanotechnol.,* 2014*,* **9**, 187–192

27. B. Wang, X. Li and L. Zhi*, ACS Nano*, 2013, **7**, 1437–1445

28. S. H. Ng, J. Wang, D. Wexler, K. Konstantinov, Z. P. Guo and H. K. Liu, *Angew. Chem. Int. Ed.*, 2006, **45**, 6896 –6899

29. J. H. Warner, A. Hoshino, K. Yamamoto, R. D. Tilley, *Angew. Chem.*, 2005, **117**, 4626-4630

30. C.K. Chan, R. Ruffo, S. S. Hong and Y. Cui, *J. Power Sources,* 2009, **189**, 1132−1140

31. M.N. Obrovac and L.J. Krause, *J. Electrochem. Soc.*, 2007, **154**, A103-A108

32. S. D. Beattie, D. Larcher, M. Morcrette, B. Simon and J.-M. Tarascon, *J. Electrochem. Soc.*, 2008, **155**, A158-A163

33. S. K. Martha, J. O. Kiggans, J. Nanda and N. J. Dudney, *J. Electrochem. Soc.*, 2011, **158**, A1060-A1066

34. S. K. Martha, N. J. Dudney, J. O. Kiggans and J. Nanda, *J. Electrochem. Soc.*, 2012**, 159**, A1652-A1658

35. M. Rinaudo*, Prog. Polym. Sci*., 2006, **31**, 603–632

36. P. K. Dutta, J. Dutta and V. S. Tripathi, *J. Sci. Ind. Res.*, 2004, **63**, 20-31

37. L. Chai, Q. Qu, L. Zhang, M. Shen, L. Zhang and H. Zheng, *Electrochim. Acta,* 2013*,* **105**, 378–383

38. L. Yue, L. Zhanga and H. Zhong, *J. Power Sources,* 2014, **247**, 327-331

39. X. Qu, A. Wirsén and A.-C. Albertsson, *Polymer*, 2000, **41**, 4589–4598

40. Hydrogel Sensors and Actuators , Editors: Gerlach, Gerald, Arndt, K.-F. (Eds.)

41. Y. Lu, W. He, T. Cao, H. Guo, Y. Zhang, Q. Li, Z. Shao, Y. Cui and X. Zhanga, *Sci. Rep.*, 2014, **4***,* 5792

42. L. An, T.S. Zhao and L. Zeng, *Appl.Energy*, 2013, **109**, 67–71

43. N. A. Choudhury, Y. Sahai and R. G. Buchheit, *Electrochem. Commun.,* 2011, **13**, 1-4

44. J. Liu, Q. Zhang, Z.-Y. Wu, J.-H. Wu, J.-T. Li, L. Huang and S.-G. Sun, *Chem. Commun.*, 2014, **50**, 6386-6389

45. H. Wu, G. Yu, L. Pan, N. Liu, M. T. McDowell, Z. Bao and Y. Cui *Nat. Commun.,* 2013, **4**, 1943

46. X. Yu, H. Yang, H. Meng and X. Xu, *ACS Appl. Mater. Interfaces*, 2015, **7**, 15961-15967

47. J. Klett, R. Hardy, E. Romine, C. Walls and T. Burchell, *Carbon*, 2000, **38**, 953-973